Estuarine, Coastal and Shelf Science 326 (2025) 109506

Contents lists available at ScienceDirect

Estuarine, Coastal and Shelf Science

journal homepage: www.elsevier.com/locate/ecss

Reef-scale variation in larval supply and settlement: validating Lagrangian dispersal predictions with observations of coral larvae

Robert A.B. Mason [a,1,*], Clothilde Langlais [b], Julian Uribe-Palomino [a], Mark Tonks [a], Frank Coman [a], Severine Choukroun [c,d], Javier Porobic [b], Christopher Doropoulos [a]

[a] CSIRO Environment, 306 Carmody Road, St. Lucia, Queensland, 4072, Australia
[b] CSIRO Environment, Castray Esplanade, Battery Point, Tasmania, 7004, Australia
[c] Centre for Tropical Freshwater Research, James Cook University, Townsville, Queensland, 4811, Australia
[d] CSIRO Environment, Australian Tropical Sciences and Innovation Precinct, Townsville, Queensland, 4811, Australia

ARTICLE INFO

Keywords:
Dispersal
Restoration
Coral reefs
Mass spawning
Model validation
Hydrodynamics
Lagrangian particle tracking

ABSTRACT

Population persistence and recovery in marine systems is driven by larval dispersal in the water column, generating ecological connectivity between the natal and settlement locations. Connectivity modelling is commonly utilised for the spatial planning of marine protected areas and, more recently, for the prioritisation of restoration interventions. Here, we conducted field experiments to validate the spatial patterns and rates of larval arrival as simulated by a high-resolution connectivity model (~300 m resolution), using complementary spatial and temporal sampling of coral larvae and newly settled recruits around a cluster of offshore coral reefs. At the within-reef scale, Lagrangian dispersal modelling demonstrated only a fair performance at predicting observed spatial patterns of larval arrival and settlement, at best. However, at the reef cluster level, hydrodynamically-driven interannual variations in larval supply were well correlated with observed interannual variations. Combined, the model results resolve empirical observations for the temporal (inter-annual) and spatial scales relevant to meta-population dynamics (1–10s of km's). At the finer spatial scales of resolution (>1/10 ha to <10 ha), relevant to current restoration interventions, skill at predicting larval density is poor whilst skill at predicting larval settlement is fair. Overall, our findings identify the need for a model validation framework that considers the scales of physical processes resolved by the hydrodynamic modelling, spatial-temporal variability in the propagule populations being measured, the error tolerance for how the outputs of model simulations are being utilised (theoretical *versus* operational), and the complementary use of modelling and field sampling for different scales of application.

1. Introduction

Understanding dispersal of passive particles by ocean currents is of broad importance to the study of marine geoscience (van Sebille et al., 2018), coastal engineering (Luo et al., 2021), fisheries (McCarroll et al., 2021), biosecurity (Beletsky et al., 2017), and ecology and evolution (Cowen and Sponaugle, 2009). Metapopulation connectivity network modelling utilises dispersal models to predict the source-sink relationships of gametes of broadcast-spawning marine fish and invertebrates, with applications to understanding the ecology, conservation, and restoration of marine reef ecosystems (Doropoulos and Babcock, 2018; Figueiredo et al., 2022; Quigley et al., 2019; Shaver et al., 2022). Marine management and conservation initiatives are increasingly incorporating connectivity modelling of marine spawners into spatial planning (Bode et al., 2024; Cecino and Treml, 2021; Faryuni et al., 2024; Rossi et al., 2014).

A key challenge in applying metapopulation connectivity networks for operational decision-making is understanding the quality of the connectivity data. Connectivity of marine species possessing pelagic larvae is driven by hydrodynamic processes occurring across a range of scales of time and space, constrained by ecological factors such as settlement competency (Cowen et al., 2007). To cover broad spatial and

* Corresponding author.
E-mail address: robert.mason@csiro.au (R.A.B. Mason).
[1] Current address: Coastal and Regional Oceanography Laboratory, Centre for Marine Science and Innovation, University of New South Wales, Kensington, New South Wales, 2052, Australia.

https://doi.org/10.1016/j.ecss.2025.109506
Received 2 February 2025; Received in revised form 20 July 2025; Accepted 18 August 2025
Available online 21 August 2025

temporal scales that range from m's to 100's km and hours to months, hydrodynamic and Lagrangian-based modelling of connectivity are required. Whilst hydrodynamic models are relatively mature at the scales of long-distance dispersal (Klingbeil et al., 2018), extending these tools to holistic models of coral larval dispersal remains a challenge due to complex physiology during long pelagic durations, and the impacts of fine-scale behavioural and physical processes (Abdul Wahab et al., 2023; Grimaldi et al., 2022; Randall et al., 2024). Incorporating all biophysical processes impacting on connectivity into modelling is challenging due to the computation required, the difficulties of making accurate parameterisations, knowledge gaps that prevent determination of an appropriate model structure for some processes, and the challenges of understanding larval dispersal and settlement (Gawarkiewicz et al., 2007; Swearer et al., 2019).

Connectivity predictions need to be pertinent for the scale at which they will be applied. The ocean processes that can impact larval dispersal and connection between reefs include tidal currents, buoyancy-driven currents, wind influence, fronts, jets, and others (Leichter et al., 1998; Werner et al., 2007). At the scale of entire reef systems, connectivity prediction using ~1–4 km resolution hydrodynamics is appropriate for planning responses to outbreaks of pests that propagate throughout the entire system (Hock et al., 2016).

However, at finer scales (<1 km) within a reef, localised circulation patterns can be difficult to model or may remain entirely unresolved. Fine scale bathymetry – gross geomorphic features unresolvable at the mapped resolution, along with the finer scale rugosity of the benthos – can lead to misrepresentation of boundary layers and turbulence in hydrodynamic models (e.g. Rogers et al., 2017). Wave pumping interacts with local bathymetry and far field currents to further modify local currents (Gourlay and Colleter, 2005). These fine scale processes can generate oceanographic features vital to understand and correctly quantify within-reef connectivity and natal-reef retention of larvae ("self-retention") (Grimaldi et al., 2022).

Decisions regarding allocation of management effort within local areas require both knowledge of connectivity between reefs and knowledge about optimal areas to restore within a contiguous patch of reef (Doropoulos and Babcock, 2018). The latter require connectivity predictions with resolutions below 500 m and accurate representation of retention (Saint-Amand et al., 2023), a scale at which models have typically remained untested.

Comparison of dispersal models with empirical data is vital to assess accuracy of predictions at the scale of their intended use. Validation of predictions from connectivity models has been undertaken through several methods. The first is direct validation of connections between source and sink nodes. This method has been performed through geochemical tracers in calcified components of organisms (e.g. Mediterranean mussel: Nolasco et al., 2018); other methods include chemical tagging of larvae (e.g. fish: Almany et al., 2007), and genetic provenance analysis (e.g. coral: Baums et al., 2006; Brazeau et al., 2005; Wood et al., 2016; fish: Bode et al., 2019), A second approach examines the spread of organisms expanding into a novel range – such as invasive fish and molluscs – and compares this to predictions of spread made with connectivity models (Beletsky et al., 2017). A third connectivity model validation method – "propagule census" – compares field-surveyed densities of larvae, settlers or recruits of the target organism to predictions from connectivity models (e.g. coral: Doropoulos et al., 2022; Golbuu et al., 2012; Gouezo et al., 2021; Oliver et al., 1992; Thomson et al., 2021; lobster: Ramirez-Romero et al., 2023). This latter approach, of the three, is the most practical for broadcast-spawning corals due to the availability of tools for assessing larval and settler densities, and due to large adult population sizes obstructing genetic or chemical tagging approaches.

In this study, we perform a validation of the spatial patterns of larval arrival within and among reefs as modelled by a marine larval connectivity model, using broadcast spawning corals as a case study. We include the following robust attributes in our modelling: (1) hydrodynamic modelling is conducted at a high resolution (305 × 305 m) compared to those typically used (>1 × 1 km); (2) sufficient particles are released per source location, at or above the seeding levels found to be robust in previous connectivity modelling sensitivity studies (Schlaefer et al., 2022; Simons et al., 2013); (3) particles are only released from areas that plausibly contain spawning populations based on recent mapping (Lyons et al., 2020; Roelfsema et al., 2021); (4) particles are released during known coral spawning windows, or windows that have been reasonably predicted when not directly observed (*vis a vis* only 13 % of prior studies); and, (5) particle release is scaled to area of habitat at release site (*vis a vis* only 16 % of prior studies). These features address the major experimental design shortcomings found in a recent review of three decades of marine connectivity modelling studies by Swearer et al. (2019).

We used a cluster of reefs on the eastern Australian continental shelf for connectivity model validation – the Capricorn Bunker region of the southern Great Barrier Reef (GBR). The Capricorn Bunker region is geographically separated from the rest of the GBR, and the size of this region allows high-resolution modelling of connectivity whilst still allowing for almost all potential source reefs to be encompassed in the domain. The region is contained within a distinct part of the oceanographic regime of the GBR, influenced by the East-Australian Current flowing from GBR waters to the north of the Capricorn Bunker region in most years, and containing an intermittent mesoscale eddy, the Capricorn Eddy (Zhibing et al., 2022). The Capricorn Bunker region contains platform and lagoonal-platform reefs whose interior are covered by water at all or some parts of the tidal cycle (Jell and Flood, 1978) (Videos 1 and 2). This feature may result in quantitative differences in self-retention and different circulation patterns, compared to reefs fringing continental islands, atolls, and barrier reefs. The Capricorn Bunker reefs are therefore a good study system of connectivity in systems of platform and lagoonal-platform reef systems worldwide.

To validate the ability of connectivity modelling to represent patterns of larval supply and retention at the reef-scale, we first compare the underlying hydrodynamic model to data from *in situ* oceanographic instrumentation, and then compare particle tracking predictions against coral larval densities measured in the water column and newly settled coral recruit (hereafter, "settler") densities on tiles deployed on the benthos. This "propagule census" approach has been used in only a handful of past connectivity validation studies at individual reefs (Oliver et al., 1992; Andrews et al., 1988; Black, 1988) or reef groups (Doropoulos et al., 2022; Gouezo et al., 2021; Thomson et al., 2021), and is unique among connectivity validation approaches in directly measuring demographically relevant larval influx. Unlike genetic, chemical tagging or geochemical methods, the field component of propagule census does not directly identify the source population(s) of individual propagules. However, source population is taken into account in the modelling, where the emphasis is placed on obtaining the best possible integration of all processes likely to affect the final larval quantity arriving at a sink reef. Connectivity model validation through propagule census is thus a validation of the end result of several consecutive models: ocean dynamics, source population productivity, particle advection, and larval ontogeny.

We generate regional supply predictions for planktonic coral larvae as well as newly settled coral recruits by applying larval mortality equations to both stages, and competency equations to the larval settlement predictions. Through modelling larval supply at small sink polygons (305 m width) co-located with settlement tile locations (ca. 10 m diameter) and plankton tow stations (ca. 100 m length), we aimed at reproducing the experimental set-up *in silico*. Our approach specifically studies the connectivity of larvae from the reef scale (sources) to the within-reef scale (sinks). Our specific aims are to:

(1) Test the ability of connectivity simulations based on a high-resolution, regionally-focused hydrodynamic model to predict

spatial patterns of propagule supply to sub-reef-scale areas from surrounding reefs, in comparison to field measurements;

(2) Explore sources of variability – environmental and biological – that may impact on the accuracy of propagule census as a connectivity measure;

(3) Perform modelling sensitivity tests to understand how mortality and competency assumptions, and the dimensions of *in silico* polygons used to represent sink locations, influence connectivity predictions.

2. Methods

2.1. Connectivity modelling

2.1.1. Domain selection

Because this study aimed to validate larval arrival predictions at distinct within-reef locations ("sinks"), we required a hydrodynamic model that encompassed all reefs ("sources") contributing larvae to those sinks. In the Great Barrier Reef, individual reefs are typically one to several tens of kilometres in size whilst distinct areas within a reef can be differentiated on geomorphic and/or hydrodynamic grounds at the scale of >1/10 ha to <10 ha ("within-reef" scale). To estimate the necessary geographic extent of the model domain, we used data from the GBR-wide connectivity study by Hock et al. (2019). Their study used the eReefs GBR4 (4 km grid) model (Steven et al., 2019) to assess between-reefs connections at the scale of the entire GBR. We identified the source reefs in the years 2008, 2010, 2012, and 2014–2016 that supplied 90 % of particles to Heron Reef, Wistari Reef and Sykes Reef – the three reefs we visited in the field – as well as to the nearby One Tree Island Reef. In all years apart from 2014, source reefs were restricted to the Capricorn and Bunker Groups, shoals immediately to the north and south, and Lady Elliot Reef (Supporting Information Data file S1). In 2014, the Swains complex of reefs contributed many source reefs.

The final domain (Fig. 1a) was selected based on the observation that most demographically relevant sources were restricted to the Capricorn and Bunker Groups, as well as the computational limits of grid size and resolution imposed by the hydrodynamic model. We refer to the three sink reefs that we focus on from hereon – Heron, Wistari and Sykes Reefs – as the central Capricorn Group.

2.1.2. Hydrodynamic modelling

The hydrodynamic model is based on the Sparse Hydrodynamic Ocean Code (SHOC) within CSIRO's Environmental Modelling Suite (EMS) (Baird et al., 2020) (Videos 1 and 2). The model uses a z vertical coordinate system (depths of vertical layers are specified in Supporting Information Table S1) and a regular horizontal grid with a cell size of 305 × 305 m.

Open ocean boundary conditions are provided to the high resolution model through a series of three nested models: the global 1/10° OceanMaps ocean model (Schiller et al., 2020) is used at the boundary of a regional Southern GBR model, which is then nested into an intermediate model before reaching the local high resolution model. Atmospheric forcing is provided by the ACCESS-R atmospheric model (Puri et al., 2013). Model outputs were saved every 12 min. Hydrodynamic hindcasts were performed for November 4, 2021–January 29, 2022 and for October 31, 2022–January 14, 2023. The hydrostatic approximation used by SHOC may not fully resolve some aspects of hydrodynamics occurring on coral reefs, such as flow over some shallow areas, and phenomena resulting from density differences generated by warm, hypersaline water creation on the reef flat.

2.1.3. Lagrangian particle simulation

Lagrangian particle dispersion was performed on hydrodynamic model outputs using Connie, a software for hydrodynamic particle advection (Condie et al., 2012). We ran Connie as a MATLAB executable (Connie version: main_tracking_connie_web_R2021a_27012022), called from within a set of Python wrapper scripts that managed input variables and output files. All runs were performed on a high-performance computing cluster.

At our 17 source reefs, design of polygons was based on areas habitable by corals in each source reef, classified as containing "coral/algae" in the benthic maps of the GBR Reef Explorer (Roelfsema et al., 2021) (Supporting Information Data file S2). Particle release timings from each source reef polygon were based on the nights we observed spawning to occur during fieldwork in November 2021 and December 2022 (Supporting Information Table S2). For November 2022, we were

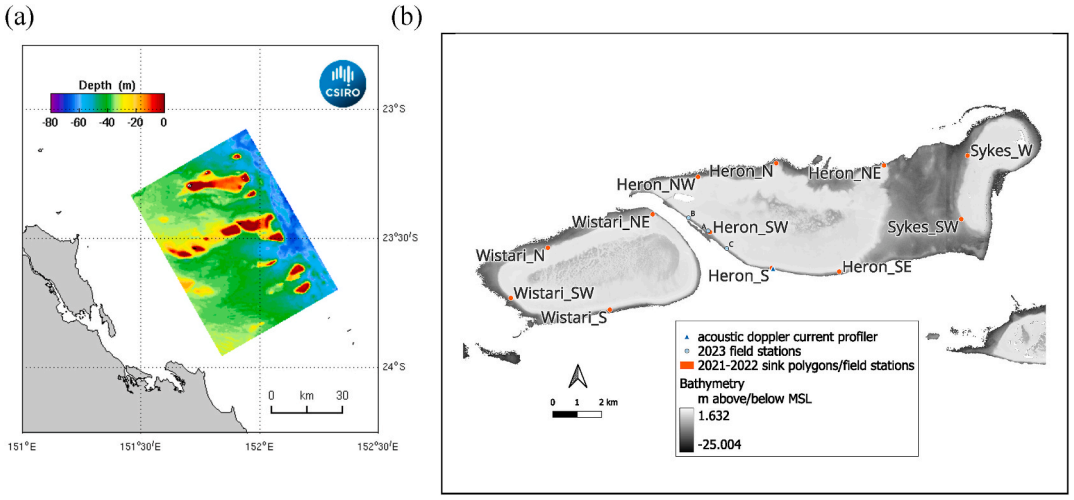

Fig. 1. (a) Bathymetry of the EMS/SHOC hydrodynamic model (tilted rectangle) covering the Capricorn Group, southern Great Barrier Reef. The selected model domain was a rectangle tilted −30° off true north that encompassed the Capricorn Group of 17 reefs (Heron, Wistari, Sykes, One Tree Island, Irving, Polmaise, Masthead, Erskine, North, Tryon, North West Island, Broomfield, Wilson Island, Wreck Island, Lamont, Fitzroy and Llewellyn Reefs). The Bunker Group (Lady Musgrave, Boult, Hoskyn and Fairfax Reefs) immediately to the south was not included in the model domain. (b) A subset of domain showing locations of the twelve field stations at Wistari, Heron and Sykes Reefs during the 2021 and 2022 spawning events, which were also the locations of the sink polygons for modelling. Locations of the three field stations during the 2023 spawning event are also shown. The location of the acoustic doppler current profiler measurements used in ground-truthing of the hydrodynamic model is indicated by the triangle. Drag-tilt current sensors were located at each of the sampling stations, except for Heron_S. The bathymetry layer is the 10 × 10 m resolution EOMAP bathymetry from the Great Barrier Reef Marine Park Authority (Creative Commons – Attribution 4.0 International License). MSL, mean sea level.

not in the field to make observations, so we instead inferred probable spawning dates following the full moon from November 2021 field observations. On each particle release date, we released 1000 particles per source reef per hour between 6 p.m. and 10:59 p.m. The initial spatial position of each particle within its source polygon, and time of release within the hour, were randomised. At release, the particles ("newly spawned coral gametes") were treated as positively buoyant and immediately resident at the sea surface. The possibility of advection or dispersion during the period of time when egg-sperm bundles float to the surface after release by adult colonies was ignored as this period is typically short (Babcock et al., 1986). To mimic the gradual sinking behaviour of coral larvae following fertilisation and initial development at the surface (Tay et al., 2011), particles remained at 0–0.5 m depth for 12 h, then 1.6–2.3 m depth for 24 h, before going to 4.0–5.0 m depth for the remainder of the dispersal period. Windage during the dispersal phase closest to the surface was set at 3 % of the wind field at 10 m height – a commonly-used *ad hoc* choice – and at 0 % during the deeper phases. Particle tracking used 120 timesteps per day and each integration through time was broken up into 10 sub-steps. Dispersal runs were continued until the date that field observations ended or the date hydrodynamic runs ended, whichever was sooner.

The use of wetting and drying processes and a z vertical coordinate system presents the issue that a surface grid cell can become dry: the lower boundary of the uppermost layer(s) can be shallower than the low-tide mark, such that they have zero thickness at low tide ("emersion") (Kleptsova et al., 2010; Lin and Falconer, 1997). To prevent computational issues, SHOC sets the current velocity values in affected layer(s) to the most recent values prior to emersion, until the tide rises above the layer's lower boundary. In many cells, emersion of the uppermost layer did occur during the first phase of dispersal, when particles were at the surface. However, this affected an average of only 77 min (range: 0–192 min) of the 732 min surface period, and mainly affected the western side of the model domain (Supporting Information Video S1). We expect the inaccurate current velocity fields experienced by particles during this brief exposure to have added only minor noise to the Lagrangian particle tracking results.

2.1.4. Selection of sink polygon locations/field sampling stations

To select sites for validation of connectivity modelling predictions using field-measured propagule abundances, 26 sites distributed around the circumferences of Heron Reef, Wistari Reef and Sykes Reef were initially evaluated. Using a hindcast of hydrodynamics for the 2015 coral spawning event, connectivity to a 200 m diameter circle placed at each of the 26 sites was determined. From these sites, a final set of 12 sites were then selected to represent a wide range of predicted connectivity as well as the geomorphic variation present among the three reefs (Fig. 1b).

2.1.5. Weighting the evening of release

The contribution of each evening to total spawning within one month was weighted to simulate the typical occurrence of one or more spawning evenings with large releases preceded and/or followed by spawning evenings with small releases (Supporting Information Table S2). For November 2021 and December 2022 these weightings were based on our field observations in the Capricorn Group, whilst November 2022 weightings were based on the November 2021 field observations.

2.1.6. Applying competency and mortality rates

Mortality of coral larvae and competency (ontogenetic readiness to metamorphose into a benthic-attached settler) as a function of time following spawning were applied to particles using the piece-wise equations of Moneghetti et al. (2019), developed for *Acropora tenuis*. Mortality and competency functions for other coral species were assessed in the sensitivity analyses (see below).

2.1.7. Assessing particle arrival at virtual field stations

For each sampling station, particle arrival was assessed at the model grid cell ("sink polygon") that, of those grid cells intersecting with the upper reef slope, was the closest one to the sampling station. The number of timesteps that a particle spent inside a sink polygon was summed. Particles were weighted by the relative size of their source reef, scaled to between 0 and 1 through dividing by the size of the largest source reef. Absolute sizes were first determined from the area of coral and algae on each reef, as mapped in the Allen Coral Atlas (Lyons et al., 2020). Sums of the timesteps spent inside sink polygons and weighting values were then used to calculate the degree of connectivity between each source reef and sink polygon. A final relative value of incoming connectivity of each sink polygon was derived by summing the pair-wise source-sink connectivity values at each sink polygon. The local spatial variation in connectivity values is the characteristic that we aimed to validate.

2.1.8. Validation of the hydrodynamic model

Hindcast velocity fields for November 2021–January 2022 and November 2022–January 2023 periods were compared to depth-averaged current measured by an acoustic doppler current profiler (ADCP), mounted on the sea floor at 13 m depth at the southern reef front of Heron Reef. Hindcasts were also compared to drag-tilt current sensors deployed at each of the 12 field sampling stations.

The metrics used in validation differed slightly for the two types of instrumentation. Drag-tilt sensors have separate measurement mechanisms for current speed and current direction, each with their own causes of error. Current speed and direction calculations were therefore separately evaluated against the equivalent outputs from the model for each drag-tilt sensor. Measurement of both speed and direction by ADCP is based on acoustics, allowing robust use of metrics that combine the two elements in model validation. We used vertically-averaged eastward and northward seawater velocity to compare outputs of the hydrodynamic model with ADCP measurements. Both types of instruments are greatly affected by the surrounding bathymetry.

2.2. Field measurement

2.2.1. Setup of field sites

Arrays of unglazed ceramic settlement tiles (11 × 11 cm, "red/yellow cobble") were installed prior to each spawning event as a means to observe coral settlement rates, using the direct attachment method of Mundy (2000). Tiles that had been used in previous deployments were cleaned in mild acid to remove any residual coral skeletal material. Fifteen plates were installed at 5–7 m depth at each of the 12 sampling stations, over 18–24 November 2021 (for spawning following the November 19, 2021 full moon), 1–6 September 2022 (for spawning following the November 8, 2022 full moon) and 8–10 December 2022 (for spawning following the December 7, 2022 full moon). For the November 2021 and December 2022 events, settlement plates were conditioned for 2–3 months at a high-flow reef slope location (4 m depth), then gently scrubbed before installation. For the November 2022 event, settlement plates were installed two months in advance so that conditioning occurred in their installed locations. One drag-tilt current sensor (Marotte HS, Marine Geophysical Laboratory of James Cook University, Townsville, Australia) was installed at each sampling station.

2.2.2. Time-series of larval arrival, 2021 and 2022

Plankton tows were conducted at each sampling station several days prior to spawning (as a baseline) and then daily for 10–12 days commencing after the first night of spawning for the November 2021 and December 2022 spawning events. Tows were conducted from a 5.9 m or 6.5 m powered vessel at low speed (1.5–2 knots) (Tonks et al., 2023). A plankton tow net with mouth diameter of 50 cm, a length of 150 cm, and a mesh size of 200 μm was used (Allied Filter Fabrics,

Berkeley Vale, Australia). Volume filtered was measured with the aid of a flowmeter attached to the bridle (Hydro-Bios, Kiel-Altenholz, Germany), with a target of 16–20 m^3 per cast. Depth of tows averaged 2.3 m, measured during the December 2022 series of tows with a depth logger attached to the bridle (Cera Diver, van Essen Instruments, Delft, The Netherlands). Tow samples were kept on ice immediately following collection and were analysed later that day. Tow contents were sorted under dissecting microscope to identify and count coral larvae. Coral larvae likely to have come from brooding species, identified on the basis of a larger size, morphological features, and presence of zooxanthellae, were excluded from the final counts. The average larval density across all days in a timeseries at a site was utilised for comparison with modelled predictions.

2.2.3. Highly-replicated measurement of larval arrival

To understand the error associated with using a single daily time point to construct timeseries of larval abundance, a separate experiment was performed (November–December 2023) to explore within-tide and within-day variation in larval densities as assessed by plankton tows. Three replicate tows were performed on each of an incoming and an outgoing tide for 8 days at each of three sites spaced 1 km apart along the south-west reef slope at Heron Reef. Tow method and scoring protocol were the same as for the 2021 and 2022 spawning events.

By generating all possible timeseries of single-daily tows at each of the three high-frequency sites, we explored the impact of within-day variation in larval measurements on the distribution, and therefore quality, of the metric (the mean larval abundance over a post-spawning timeseries consisting of one tow per day) used in model validation. These distributions were then compared to the mean larval abundance over *all* tows conducted at the same site ("true mean") – the closest measure of true larval abundance that we could obtain.

2.2.4. Measurement of coral settlement

After a period of several weeks from the start of the November 2021, November 2022 and December 2022 spawning events, settlement tiles were retrieved from all sites and kept immersed in a flow through seawater trough under shade. The tile retrievals occurred on 7 December 2021 (following the November 2021 event), 8–10 December 2022 (following the November 2022 event) and 24–26 January 2023 (following the December 2022 event). All coral settlers on the upper and lower surface of each tile were counted and photographed at up to 4.5× magnification using stereo microscopes. Scored settlers were categorised into spawned or brooded taxa from the photographs using a combination of size, zooxanthellae presence/absence and, when present, skeletal morphology (Babcock et al., 2003; Baird and Babcock, 2000). The average count of spawned settlers across all tiles at a site was utilised for comparison with modelled predictions.

2.2.5. High-temporal resolution larval settlement (November 2021)

To capture high resolution temporal dynamics in coral settlement, a series of four consecutive 2-day tile deployments were performed at four sites following the November 2021 spawning event. Twenty tiles attached to 25 cm lengths of threaded stainless-steel rod were deployed for 48 h at each site on 26 November, 28 November, 30 November, and December 2, 2021. Tiles were retrieved following each period and processed as described above.

2.3. Statistical analysis

Observed larval arrival (mean number of larvae m^{-3} over the timeseries at a site) and coral settlement (mean number of settlers $tile^{-1}$ at a site) were not normally distributed so were $\log_e$-transformed prior to analysis. Transformed values were pooled over all events and then fitted to predicted larval arrival or coral settlement using linear models ("gaussian" model choice in the glmmTMB R package, v. 1.1.9: Brooks et al. 2017). Observed coral settlement was $\log_e$-transformed and fitted to observed larval arrival using a linear model, with the *y* intercept forced through zero due to the clear causative relation between the two.

Larval counts from highly replicated plankton tows during November 2023 were analysed using a negative binomial model ("nbinom2" model choice in glmmTMB), with site and tide (flood/ebb) as fixed effects and distance towed ($\log_e$-transformed) as an offset.

2.4. Sensitivity analyses

Sensitivity analyses were performed to measure the impact of varying some parameters and structural elements of the Lagrangian particle tracking methods.

(i) We tested the impact of using different equations for competency and mortality. Connolly and Baird (2010) utilised a different equation structure for calculating competency and mortality to Moneghetti et al. (2019). We ran sensitivity tests using Connolly and Baird's (2010) equation set for *Acropora valida* and *Platygyra daedalea* – two common but functionally different coral species.

(ii) We conducted a sensitivity test of the impact of receiving polygon size and coverage through comparing runs from the main analysis (receiving polygons consisting of single grid cells) to runs with the receiving polygons set as 3 grid cells, 5 grid cells (both parallel to the reef perimeter), or 200 m diameter circles centred at the location each sampling station (Supporting Information Figure S1). To ensure comparability between the different sets of receiving polygons, connectivity results for each set of polygons were standardised by multiplying by the ratio of the area of the original (single grid cell) receiving polygons to the area of the respective updated set of receiving polygons.

The predicted coral settlement from each sensitivity test were then regressed against the observed settlement rates, as for the main analysis. Performance of each sensitivity analysis was assessed by comparing the R^2 value of this regression to the R^2 value of the observed *vs* modelled settlement in the main analysis (referred to as the "reference case").

3. Results

3.1. Validation of the hydrodynamic model

3.1.1. Qualitative analysis of current patterns

Animations of modelled sea-surface hydrodynamics for the model domain in December 2021 (Video 1) and November to December 2022 (Video 2) illustrate distinct patterns of salinity and thermal dynamics in the lagoons of platform reefs, compared to the surrounding waters. This suggests that the specific hydrodynamic patterns generated by the geomorphology of platform reef shallow lagoons are being appropriately captured. Circulation patterns around Heron Reef were also compared to a report of a well-validated very high-resolution model of Heron Reef (167 × 167 m) performed with the same hydrodynamic model, SHOC (Mongin and Baird, 2014). Circulation around Heron Reef in our model is anticlockwise, matching that observed in the very high-resolution model (Mongin et al., 2016).

3.1.2. Comparison of modelled flows to in situ sensors

An acoustic doppler current profiler was situated on the southern side of Heron Reef in 2021–2023 (Fig. 1b). Modelled water velocity and tides at this point were compared to measured values for every hour over the modelled periods. Modelled eastward water velocity at the grid cell containing the measurement site resolved well, being just 9.6 % greater than measured seawater velocity over the Nov 2021–Jan 2022 period (Supporting Information Figure S2) and 5.1 % greater over the Nov 2022–Jan 2023 period (Supporting Information Figure S3). Modelled northward seawater velocity did not perform as well and was 20.2 % lower than measured seawater velocity over the Nov 2021–Jan 2022

period (Supporting Information Figure S4) and 40.7 % lower over Nov 2022–Jan 2023 (Supporting Information Figure S5). As the instrument location and model grid cell are located immediately south of the rim of the Heron Reef lagoon, it is likely that there are fine-scale bathymetric controls on the northward component of current that are not fully resolved at the resolution of the model. In contrast, a relatively strong match between the model and instrument for eastward flows, occurring parallel to the reef rim with the proximal influence of the Heron-Wistari channel, suggests moderately good model approximation of flows over gentle bathymetry.

There was an extremely good fit with the timing and height of tide in Nov 2021–Jan 2022: the model *vs* instrumental measurements of sea level showed a near 1:1 match (Supporting Information Figure S6). In Nov 2022–Jan 2023 the model and measurements displayed a 3 % difference, indicating a very slight bias in the modelled tide (Supporting Information Figure S7).

A tidal decomposition analysis of the SHOC/EMS model *vs* the ADCP observations was performed, with a slight adjustment of the vertical averaging window used on modelled data to better fit that used with the observations, and a slight adjustment of the location used in the model to better reflect the bathymetry of the ADCP location. Skill scores from this analysis revealed better model performance in eastward compared to northward direction, as above (Supporting Information Figure S8 and Figure S9, top panels). Tidal currents were also represented accurately, though with a slight bias in direction compared to observations (Supporting Information Figure S8 and Figure S9, middle panels). The model also reproduced, relatively well, the low frequency circulation seen in the observational data (Supporting Information Figure S8 and Figure S9, bottom panels).

Drag-tilt current sensors located at 11 sampling stations in 2021 (Fig. 2) indicated several geographic regions where the hydrodynamic model was either performing well or under-performing. At the north-west and south-east reef slopes of Heron Reef, the northern, southern and south-western reef slopes of Wistari Reef, and the western and south-western reef slope of Sykes reef, the distribution of modelled current direction reasonably closely matched that of measured direction. At sites proximal to the Heron-Wistari channel (the south-western reef-slope of Heron Reef and the north-eastern slope of Wistari Reef), and at the north-eastern corner of Heron Reef, the modelled current directions displayed poor agreement in comparison with the measurements. At the north-central slope of Heron Reef, an area via which the Heron lagoon drains during the high-to-low tide transition, the modelled current distribution displayed lower agreement with the measurements in one leg of the tidal cycle but moderately good agreement during the opposite leg of the tidal cycle. One possibility is that the sensor was in the lee of a bathymetric feature during that leg. An analysis of modelled current speed *vs* drag-tilt measurements is presented in Supporting Information, "Comparison of modelled versus drag-tilt sensor-measured current speeds" and Supporting Information Figure S10–Figure S20.

3.2. Modelled predictions versus field observations of early life stages

3.2.1. Larval arrival

There was no significant relationship between observed and predicted larval influx across the November 2021 and December 2022 coral spawning events (Fig. 3a).

By comparing time series of the observed incoming larvae of both events, some repeated patterns were revealed (Fig. 4). Two sites at Wistari Reef had low larval influx in both events (Wistari_NE and Wistari_S) whilst the southern side of Heron Reef contained the highest influx in both events (Heron_SE in November 2021, Heron_S in December 2022). The model agrees with low larval influx at Wistari_NE and displays a relatively high larval influx on the southern side of Heron Reef.

Following the November 2021 event, larval peaks occurred 1–2 evenings after spawning (November 28 and 29) and also 6–7 evenings after the end of spawning at many sites (December 2 and 3) (Fig. 4). In December 2022, larval peaks occurred part-way through the spawning event at many sites (December 12 and 13 at some northern sites, 14 at some southern sites), and 1–3 evenings after the end of spawning (December 16 and 18) (Fig. 4).

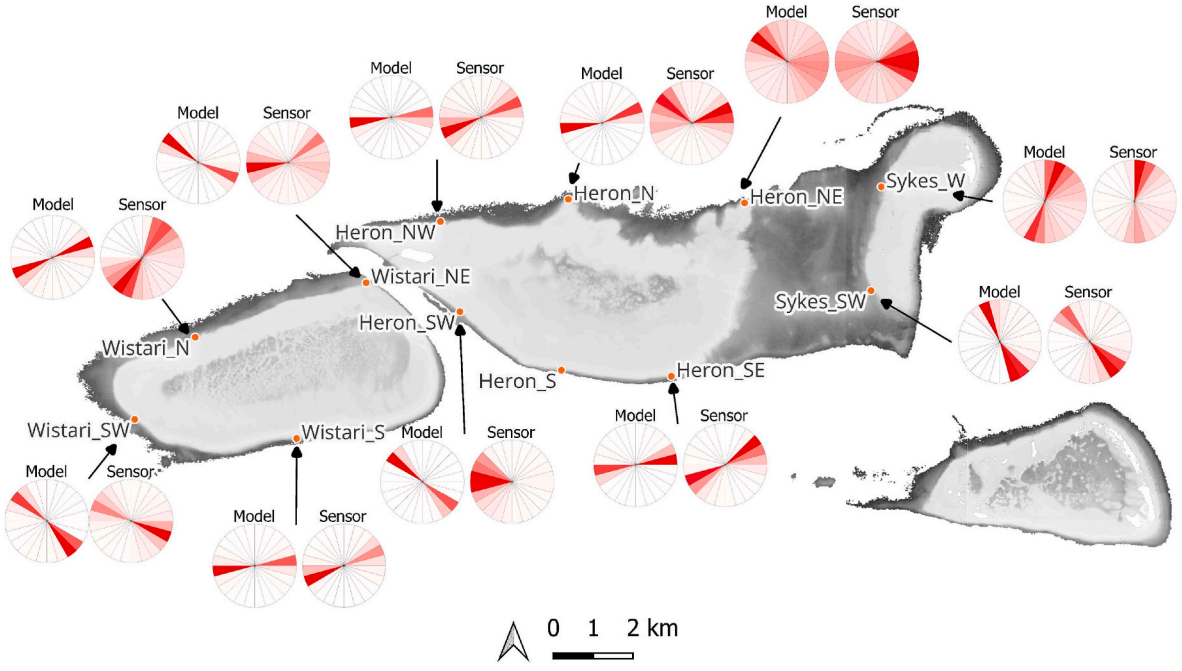

Fig. 2. Comparison of current direction from the EMS/SHOC model vs current direction measured with drag-tilt sensors at eleven sites around Wistari, Heron and Sykes Reefs in November and December 2021. Intensity of red colouration in pie chart segments indicates the proportional frequency of the current in that compass direction. For comparisons of modelled and measured current speed, see Supporting Information Figure S10-Figure S20. (For interpretation of the references to colour in this figure legend, the reader is referred to the Web version of this article.)

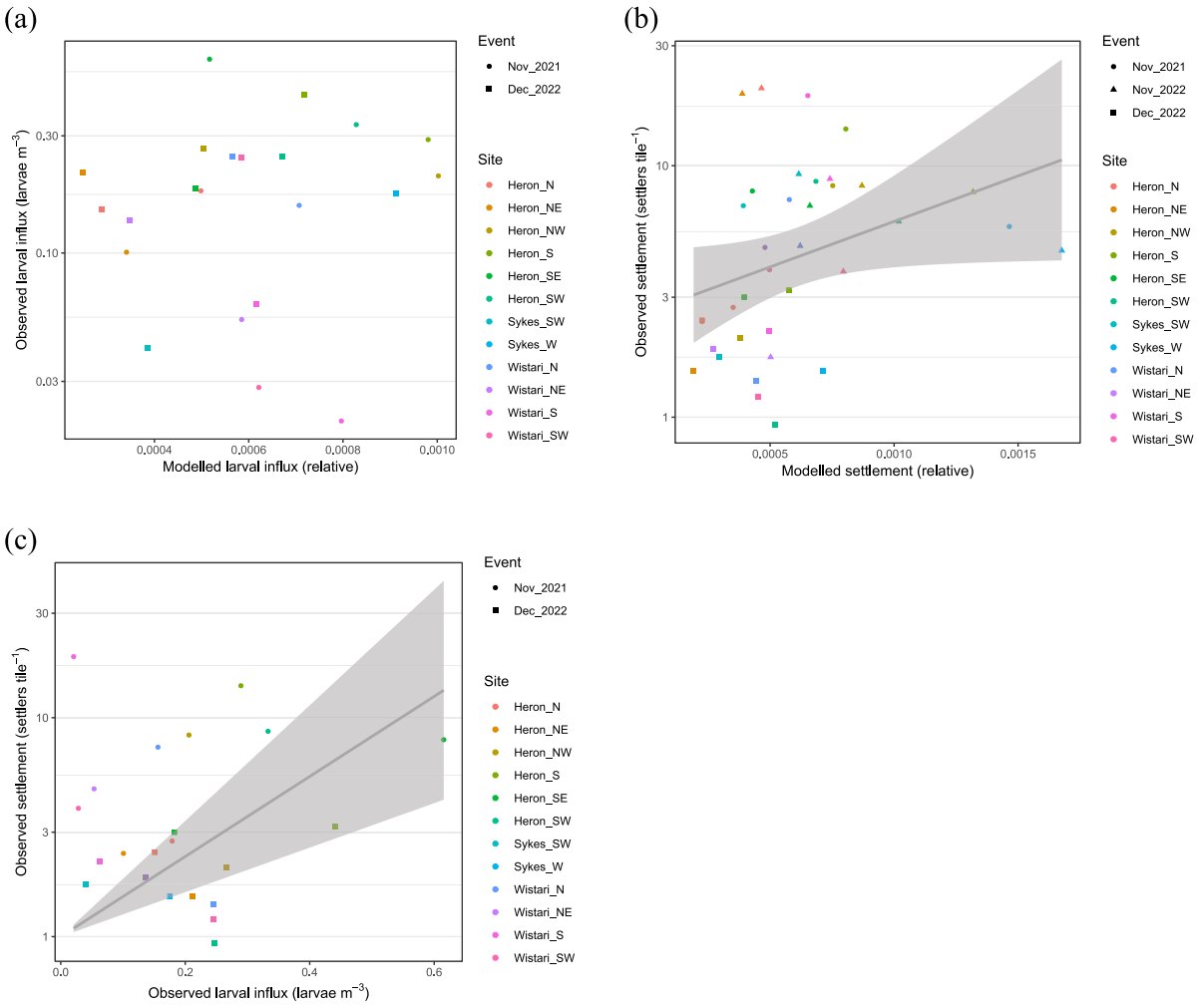

Fig. 3. (a) Observed vs modelled larval influx over two spawning events (November 2021 and December 2022). (b) Observed vs modelled coral settlement over all three spawning events. (c) Measured coral settlement vs larval influx following the November 2021 and December 2022 spawnings. In (a) and (b), modelled influx or settlement was to the model grid cell closest to each sampling station. In (b), the line is the linear regression line, for which $R^2 = 0.11$, and the grey area is the 95 % confidence interval. Observed settlement is the average number of coral settlers over n = 15 settlement tiles site^{-1} in most cases, n = 14 tiles site^{-1} for Wistari_SW in Nov. 2021 & Heron_N in Dec. 2022, and n = 12 tiles site^{-1} for Heron_SW in Nov. 2022 & Heron_N in Nov. 2022. In (c), the intercept was forced through zero due to the causative relationship between larval arrival and settlement, and the regression line had the equation: mean settlers tile^{-1} = 23 × mean larvae m^{-3}. In all three plots, the *y* axis is on a $\log_{10}$ scale.

3.2.2. Coral settlement

Across the three events, modelled settlement was significantly correlated with observed settlement on tiles deployed for several weeks following spawning (Fig. 3b, $p = 0.03$, $R^2 = 0.11$). Inclusion of the spawning event each datapoint came from as a random effect resulted in a better AIC value (76.98 with *vs* 89.73 without) but resulted in a non-significant relationship between observed and modelled settlement. Settlement was <10 settlers tile^{-1} at most sites (>80 %) during all events. A notable exception was at two adjacent sites on the northern side of Heron Reef, Heron_N and Heron_NE, where settlement was very high (~20 settlers tile^{-1}) during the November 2022 event (Fig. 5). At the southern side of Heron and Wistari Reefs (Heron_S and Wistari_S), settlement was also high (14–19 settlers tile^{-1}) during the November 2021 event. The spatial aggregation of these very high settlement events suggests a shared biophysical explanation at adjacent sites within one event. The modelled data did not predict that either set of sites should have particularly high settlement during the respective events (Fig. 6), possibly showing the existence of hydrodynamic or biophysical phenomena that are not captured by the model.

3.2.3. Larval arrival vs coral settlement

Over the November 2021 and December 2022 events, observed coral settlement displayed a significant relationship with observed larval arrival ($p < 0.001$, $R^2 = 0.26$) (Fig. 3c). Inclusion of the spawning event that each datapoint came from as a random effect resulted in a non-significant relationship between observed and modelled settlement.

Modelled larval arrival and modelled coral settlement differ only by the inclusion/exclusion of a mortality function. We found that this difference in model structure made little practical difference, as the modelled larval arrival and modelled coral settlement were highly correlated ($R^2 = 0.987$; slope $p < 0.001$; y-intercept not significant) (Supporting Information Figure S21), and the modelled predictions are on a relative, not absolute, scale. We use this as a justification for using modelled settlement as a proxy for modelled larval supply in the spatial comparisons of the next section.

3.3. Spatial and temporal patterns of larval supply

3.3.1. Sectors of predicted larval supply

The connectivity model produced consistent spatial patterns within the individual reefs across spawning events (Fig. 6). For Heron Reef,

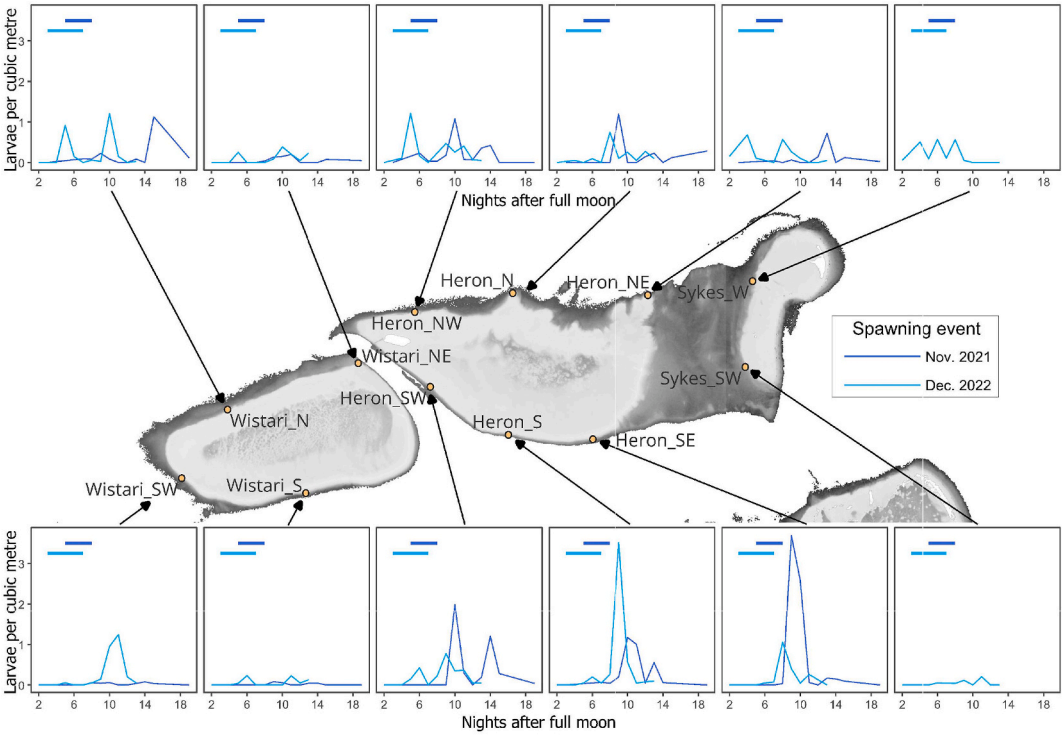

Fig. 4. Observed larval influx following the November 2021 and December 2022 spawning events. The range of nights on which spawning was observed in the field during each event are indicated by the bars towards the top of each figure. Dates that correspond to nights after full moon (NAFM) are November 21, 2021 (2 NAFM) to December 8, 2021 (19 NAFM) and December 10, 2022 (2 NAFM) to December 27, 2022 (19 NAFM).

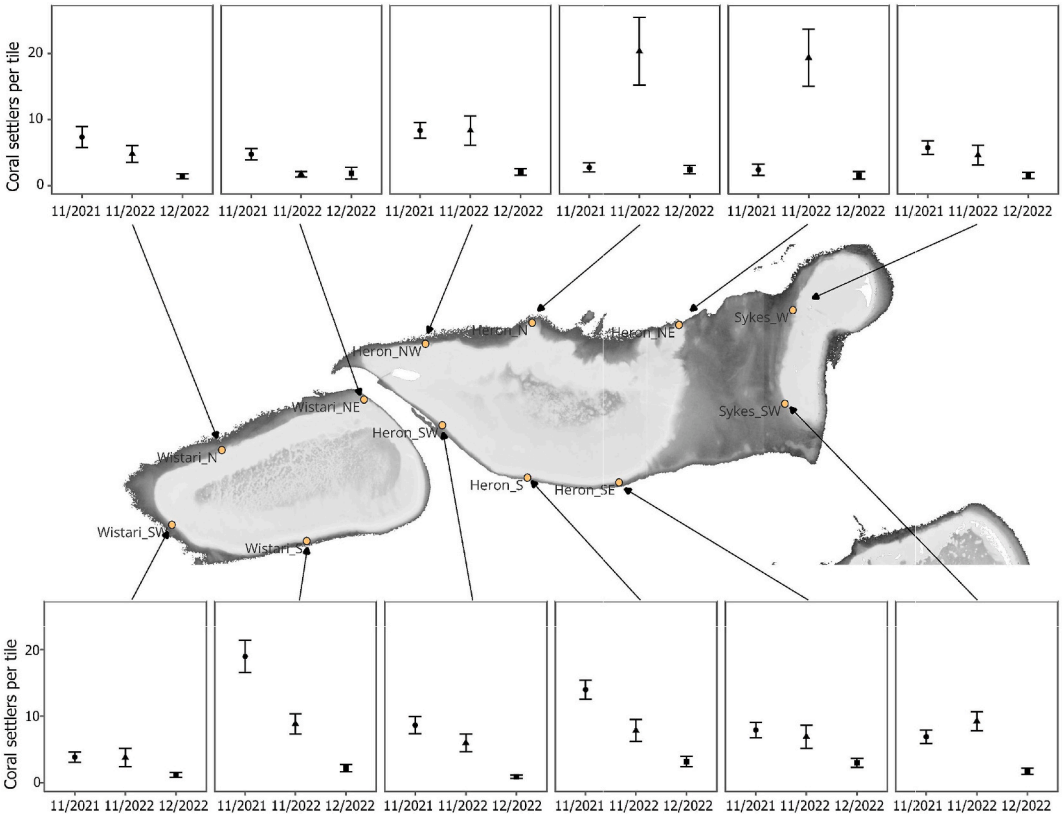

Fig. 5. Settlement at each site (mean ± SEM) following the November 2021 ("11/2021"), November 2022 ("11/2022") and December 2022 ("12/2022") spawning events.

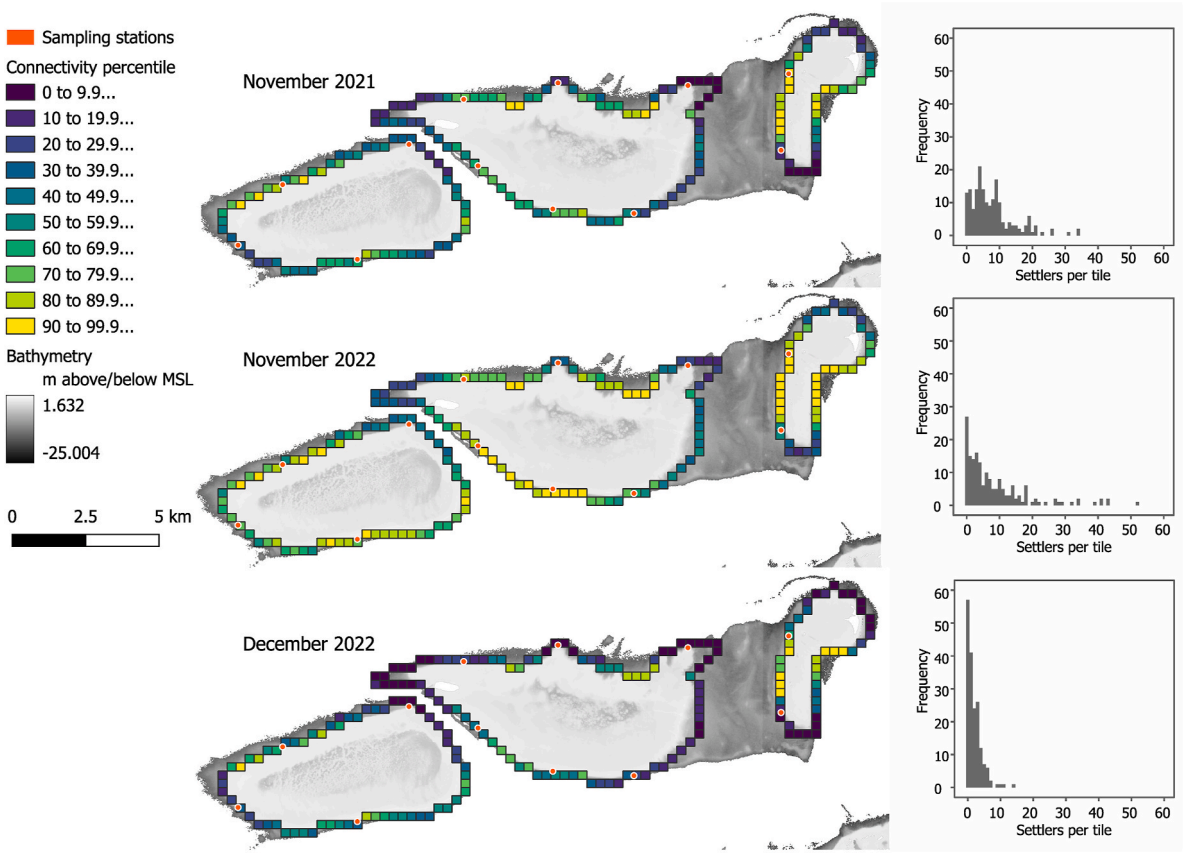

Fig. 6. Relative connectivity around the perimeters of Heron, Wistari and Sykes Reefs indicates that, in aggregate, modelled connectivity (larval settlement) following the November 2021 spawning (top left panel) was lower than that following the November 2022 spawning (middle left panel) but higher than that following the December 2022 spawning (bottom left panel). Percentile ranks are based on data pooled over all three spawning events. Panels on the right show the corresponding distribution of settlers per settlement tile over all sampling stations following the November 2021 spawning event (top right panel), the November 2022 spawning event (middle right panel), and the December 2022 spawning event (bottom right panel). Counts of coral larval settlers per tile (*x* axis) were binned into individual integers. "Frequency" on the *y* axis is the number of tiles having the corresponding count of settlers. The grid cells depicted correspond to those in the hydrodynamic model grid that intersected with the edge of each reef, based on the 2004 GBRMPA Reef Polygons. MSL, mean sea level.

higher larval supply is found in the SW and N sectors of the reef. In the N sector, high supply is consistently found in the inwards flexing parts of the reef, which create sheltering "bays" that facilitate higher retention. For Sykes Reef, higher larval supply areas are found on the eastern and western sectors of the reef, and for Wistari Reef, higher larval supply is found along the NW and SE quadrants of the reef.

3.3.2. *Qualitative validation of predicted spatial patterns*

Combining the two observed spawning events (November 2021 and December 2022) and three simulated events for the model, we compare the relative larval supply characteristics of each reef. Larval influx observations indicate that the three stations at the southern edge of Heron Reef receive higher supply overall than the 3 stations at the northern edge of Heron Reef (Fig. 4). Across the three modelled events, the three southern stations demonstrate higher predicted input than the three northern stations (Fig. 6). For Wistari Reef, both empirical and modelled datasets display high larval supply in the northern quadrant. Similarly, both display low larval supply in the south-west quadrant. The southern sector displays a relatively high supply in the model, but the station displays a relatively consistent low larval supply in observations from November 2021 and December 2021 (Fig. 4). However, coral settlement at Wistari_S is high relative to the other stations at Wistari Reef, suggesting that the plankton tows missed high larval input or retention at that site (Fig. 5). For the north-east sector of Wistari Reef, observed larval supply is relatively low to medium at the station location, and is a low larval supply sector in the model. Note that this is an area where *in situ* instrumentation suggested poor hydrodynamic model performance. For Sykes Reef, empirical observations and modelled data agree, with more larval supply in the western sector than in the south-western one.

3.3.3. *Inter-event patterns of modelled and observed settlement*

Inter-event patterns of modelled settlement across all sites reflected inter-event patterns of observed settlement. Predicted settlement over the reef slopes of the three reefs in the central Capricorn Group (Fig. 6) was lower following the November 2021 spawning event than following the November 2022 spawning event. Though there was no significant difference in observed settlement among the events under a negative binomial generalised linear model, a markedly longer tail on the right side of the distribution (more instances of very high settlement on tiles) was observed following the November 2022 event than following the November 2021 event (Fig. 6). Because the same number of particles were modelled in all three spawning events, this evidence suggests that the modelling has captured the larger scale hydrodynamic forcing(s) that drove a higher proportion of larvae towards the central Capricorn Group following the November 2022 event than following the November 2021 event. Modelled and observed larval settlement were both lower following the December 2022 event than either the November 2021 or November 2022 events (Fig. 6). This concordance may have been due to less inter-reef connectivity in December 2022 due to large scale current variability, but was most likely due to the 2022 split spawning event having a large release in the first month and, consequently, a smaller release in the second month.

3.4. Sources of variation in field measurements

3.4.1. Larval arrival vs coral settlement at high temporal resolution

In 2021, the abundance of larvae in the water column approximated, on a relative basis, the level of coral settlement in a series of four 48 h intervals, at four sites (Fig. 7). The correlation of larvae to settlers was not significant in Spearman rank tests for larvae arriving one, two, three and four days prior to the end of each 48 h settlement assessment period. However, at two sites (Heron_NW and Heron_SW), dramatic increases in settlement on 30 November–2 December and 2–4 December were preceded by, or coincided with, large pulses of larval input on 29 November and 2 or 2–3 December. At Wistari_N, mild increases over 28–30 November, 30 November–2 December, and 2–4 December were preceded by a mild pulse of larvae over 28–30 November. At Wistari_NE, a strong increase in settlement on 30 November–2 December was preceded by only a modest pulse of larvae on 26–28 November, suggesting that a pulse of larvae may have been missed in plankton tows at this site. A subsequent strong pulse of larvae on 4 November coincided with reduced (compared to the previous timepoint), but still strong, settlement on 2–4 November. The time of the larval tows on 4 November was also the time of the retrieval of the tiles and therefore the plankton values would only influence settler numbers if they were indicative of incoming larvae over the 12 h preceding the tow.

3.4.2. Highly-replicated measurement of larval arrival

A larval peak was observed between 6 and 9 December, 5+ days after the first recorded night of spawning in 2023 at three high-frequency sampling sites (Fig. 8a, c, e). On these days, replicate tows within the same leg of the tide (incoming *vs* outgoing) displayed some variation, yet the variability was inconsistent among tows in opposing tides (Fig. 8a, c, e). A negative binomial generalised linear mixed model indicated that site had a significant effect on larval count in tows ($p < 10^{-5}$; post-hoc: C = A > B). The interaction of site with tide (ebb *vs* flood) was marginally non-significant ($p = 0.0502$).

At the low larval supply site B, the distribution of the validation metric was very tight around the true mean (Fig. 8d). At site C, where a peak in larval abundance was observed from December 6, the validation metric had a much greater spread around the true mean (Fig. 8f). At site A, where an increase in larval abundance was observed from December 7 and a peak observed on December 9, the validation metric displayed a bimodal distribution around the true mean (Fig. 8b).

3.5. Model sensitivity analysis

For mortality and competency, sensitivity analyses revealed that parametrisations for the base model were more-or-less optimal. Connolly and Baird's (2010) equations for *A. valida* achieved a slightly higher R^2 value than the base reference case (Table 1, Supporting Information Figure S22b). Connolly and Baird's (2010) equations for *P. daedalea* achieved slightly lower R^2 values compared to the reference case (Table 1, Supporting Information Figure S22c). Using receiving polygons the size and position of five hydrodynamic grid cells parallel to the reef perimeter, and centred at the field sampling stations, resulted in a non-significant correlation between observed and modelled settlement (Table 1, Supporting Information Figure S23a). However, when sites at Sykes Reef, which had far larger modelled settlement than other sites, were excluded, the correlation was significant with a substantially higher R^2 value than the reference case (Table 1, Supporting Information Figure S23b). Using receiving polygons the size and position of three hydrodynamic grid cells parallel to the reef perimeter resulted in a significant correlation, with an R^2 on par with the reference case (Table 1, Supporting Information Figure S23c). Using receiving polygons that were the size of 210 m diameter discs centred at each field sampling station resulted in a non-significant correlation (Table 1, Supporting Information Figure S23d). Two sites (Heron_S and Heron_SW) had zero modelled larval arrival in both years using circular sink polygons, yet larvae were observed in the field samples. Excluding these sites resulted a significant correlation between observed settlement and modelled settlement at the circular sink polygons, with an R^2 moderately higher than the reference case (Table 1, Supporting Information Figure S23e).

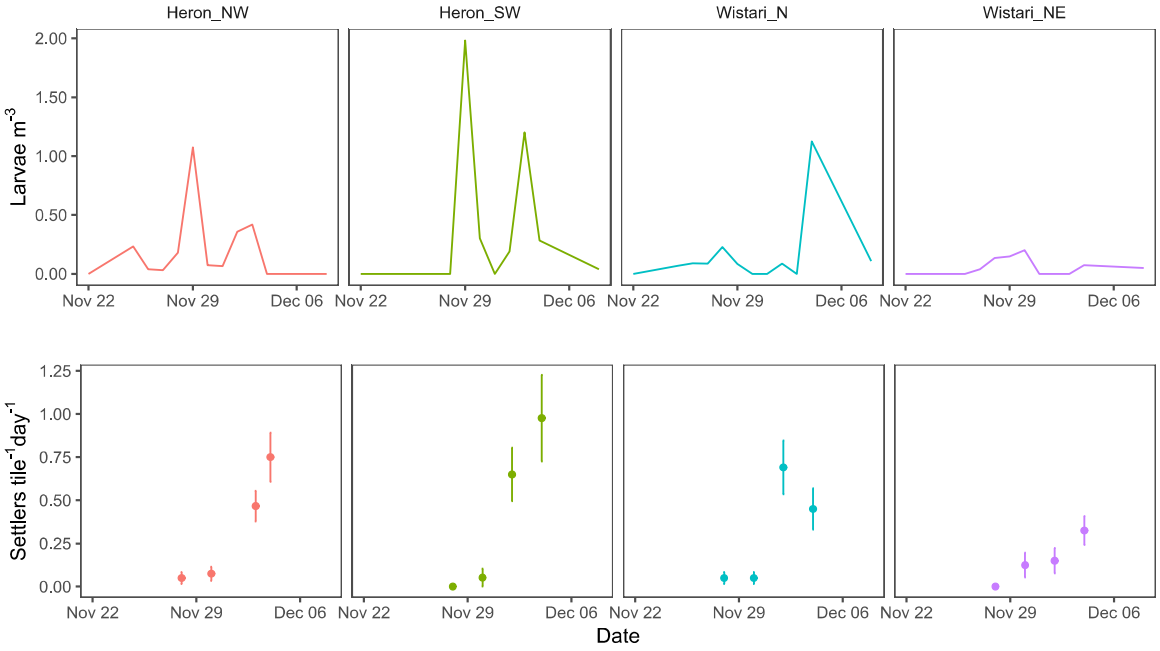

Fig. 7. Water column larval density (top row) compared to rate of coral settlement (coral settlers per tile per day) over 48 h windows (bottom row) at four sampling stations in 2021. Coral settlement rate is shown on the end date of the respective 48 h window. Settlement plates were deployed and collected mid-morning. At Heron_NW, the penultimate coral settlement datapoint was over a 36 h window and the final datapoint over a 24 h window.

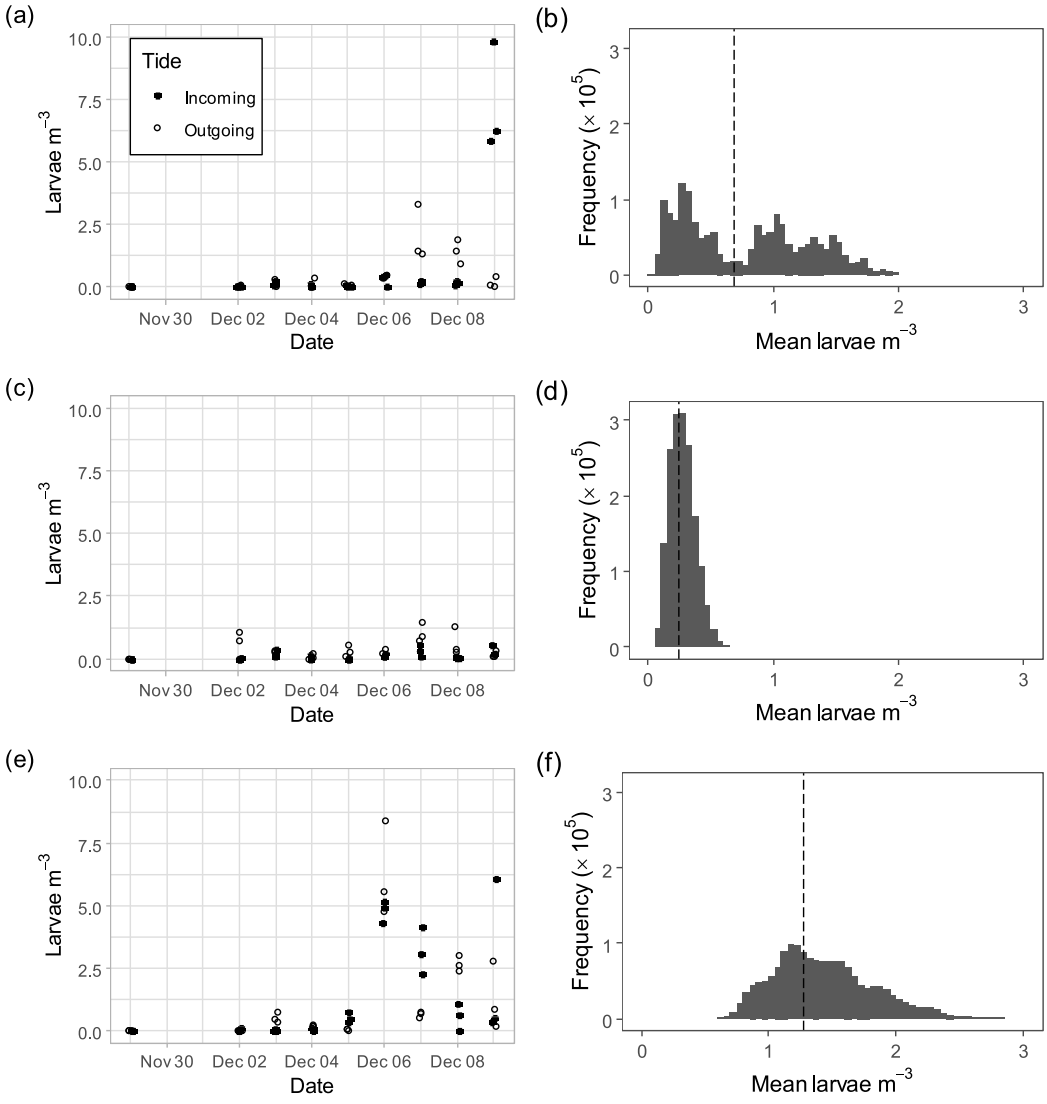

Fig. 8. Stochasticity in coral larvae water column densities was tested by performing three plankton tows on each of a rising tide and a falling tide per day at each of three individual sampling stations at Heron Reef. Panels (a), (c) and (e) depict data for, respectively, site A, site B and site C, whose locations at Heron Reef are shown in Fig. 1b. Distributions of the means of all possible timeseries of larval sampling events, generated through choosing one sampling event from the six performed per day between 2 December and December 9, 2023, are shown for (b) site A, (d) site B and (f) site C. The mean of all larval density measurements, i.e. all six plankton tows each day over all eight days, at each site in December 2023 are shown as the dashed lines.

Table 1
Sensitivity testing of key parameters and methods. All tests were performed using model reruns of the November 2021 spawning event. For reference, the parameters used in the main analysis are included (underlined).

Sensitivity test category:	Slope *p* value	R^2
Competency & Mortality		
Moneghetti et al., 2019 (*Acropora tenuis*)	0.03	0.11
Connolly and Baird, 2010 sp. 1 (*Acropora valida*)	0.024	0.126
Connolly and Baird, 2010 sp. 2 (*Platygyra daedalea*)	0.044	0.104
Changing the spatial characteristics of receiving polygons		
Single hydrodynamic model grid cell (305 × 305 m)	0.03	0.11
Closest 5 hydro-model grid cells on reef perimeter to sampling station	0.863	0.001
Closest 5 hydro-model grid cells on reef perimeter to sampling station, without sites at Sykes Reef	0.003	0.225
Closest 3 hydro-model grid cells on reef perimeter to original polygon	0.029	0.12
Circular receiving polygon (210 m in diameter)	0.194	0.046
Circular receiving polygon without Heron_SW and Heron_S	0.028	0.143

4. Discussion

Biophysical modelling is an important tool for understanding marine connectivity in contexts relevant to environmental decision making (Gawarkiewicz et al., 2007). Whilst models have limits to what they resolve, they also offer the advantage of capturing the connectivity for a range of spatio-temporal scales. Observations, in contrast, are limited in that they provide information only about specific spatio-temporal windows. However, combining modelling with observational datasets, if done robustly, provides the potential for well-validated connectivity predictions that are relevant to environmental management. We have validated the hydrodynamic outputs of a high-resolution biophysical model, and have then shown that a model of such calibre makes statistically significant, but nevertheless quite variable, predictions of coral propagule influx. Though a moderately optimistic outcome, this skill at larval supply and settlement prediction likely falls short of the requirements of some local management applications (Ladd and Burkepile, 2018) and suggests a formal framework for connectivity model validation and use is required for minimisation and management of

model error.

Observational data provide the scope to test the within-reef spatial patterns of larval supply predictions of a connectivity model that is broadly applicable to many reef areas. Physical oceanographic data from *in situ* instrumentation was first utilised to test the underlying hydrodynamic modelling. Hydrodynamic outputs of a SHOC model centred on the Capricorn Group of reefs replicated natural tidal behaviour, measured with an acoustic doppler current profiler (ADCP), extremely well. Current predictions parallel to the reef perimeter displayed a strong match up to ADCP measurements, whilst currents perpendicular to the reef perimeter displayed a moderate match to measurements. Drag-tilt sensor data allowed for hydrodynamic validation over a broad part of the model domain, covering most field sampling stations. The hydrodynamic output displayed good accuracy at most locations but moderate accuracy along the north edge of Heron reef (over which the Heron lagoon drains) and poor accuracy of current direction at sites close to the Heron-Wistari channel. A poor match between measured and modelled currents may indicate several possible issues, including the influence of fine scale local topography not captured at the resolution of the bathymetric model (Gouezo et al., 2025).

Hydrodynamic phenomena that are non-hydrostatic, wave-associated, or caused by benthic complexity may also be important to consider. A strong wave regime may generate wave setup across a platform reef, possibly becoming a dominant component of the lagoonal flow patterns experienced by larvae (Grimaldi et al., 2022). The rugosity generated by the morphological complexity of coral colonies may create flow effects through wave/porous matrix interactions (He et al., 2022). Waves may also mix surface larvae down into the water column (Willis and Oliver, 1988). Long filamentous aggregations of buoyant gametes or larvae, generated through topographically-controlled fronts, baroclinic fronts, or Langmuir circulations are, anecdotally, an important feature of coral spawning events (Oliver et al., 1992; Willis and Oliver, 1988; Alldredge and Hamner, 1980). Their role in generating reef connectivity, and the role of waves and wind in their generation, advection and degradation, has not yet been addressed in coupled hydrodynamic-Lagrangian connectivity modelling.

Methods used for validation of hydrodynamic data in other connectivity studies vary. Some other studies use individual measurement types for hydrodynamic validation including ADCP measurements (Cavalcante et al., 2020), temperature timeseries (Mongin and Baird, 2014), satellite altimetry measurements of current (Uchiyama et al., 2018), or drifters (Storlazzi et al., 2017). The degree of validation of hydrodynamic modelling against observational data in connectivity studies varies and it is performed in a minority of studies, with most studies having an underlying and unsubstantiated assumption that the hydrodynamic model is performing well.

Instrumentation data were compared to the hydrodynamic output from the model grid cell that they were "located" in. A caveat is that the position of sub-mesoscale hydrodynamic features may differ slightly between the model and real life. As such, the model might predict the feature but not its exact location – the double penalty effect (Rossa et al., 2008). The higher a model's resolution is, the more that penalties may manifest. Moreover, fine bathymetric gradients or other local features may also generate a range of hydrodynamic conditions within the area covered by a grid cell, driving differences between the modelled predictions for the grid cell and actual conditions at the sampling site. For example, an anomaly between ADCP and hydrodynamic model results beside a local topographic feature not well represented in the model was found by Bruyère et al. (2023). In our results, deviations between modelled and measured conditions were present at geomorphic features that may present challenges to accurate *in silico* replication (a narrow channel or a lagoon drainage area). This supports the proposition that model *vs* instrumentation anomalies at some sites do indeed indicate poor model performance in the surrounding area, and conversely that model *vs* instrumentation concordance at other sites indicates better model performance in those areas. As shortcomings of our hydrodynamic model appeared to be associated with only a few reef-located bathymetric features, whilst good performance was found in most other reef areas, progressing to validation of connectivity predictions was worthwhile.

Predicted settlement was correlated with our field-observed values over the three spawning events that we studied, but with high variance (Fig. 3b). Other studies have found concordance between connectivity-modelled and field-measured values for coral settlement. Andrews et al. (1988) found that modelled connectivity patterns concorded with locations of high *vs* low coral settlement at a central GBR lagoonal reef. Notably, this study used a very high-resolution (50 × 50 m) hydrodynamic model but focused on self-retention and omitted inter-reef larval transport because the model system used is a single, relatively isolated, reef. Oliver et al. (1992) found no correlation of their modelled predictions to actual coral settlement measurements in a well-mixed, mid-shelf system in the central GBR. The domain of that model did not include other reefs, however, inter-reef connectivity was coarsely simulated through seeding of particles along the model boundary. Conversely, a similar hydrodynamic model adapted for Palau generated connectivity predictions that matched field-observed coral settlement and juvenile coral densities (Golbuu et al., 2012; Gouezo et al., 2021). Thomson et al. (2021) found that observed coral settlement in north-west Western Australia was adequately predicted by moderate to high modelled connectivity together with metrics of observed coral cover and turbidity. Using the same model, Doropoulos et al. (2022) found that observed coral settlement was significantly related with modelled self-recruitment potential across a gradient of larval supply in north-west Western Australia.

In our present study, the model proved to have skill at predicting the interannual variability effect of hydrodynamic forcing on larval settlement. Both modelled and measured settlement in the central Capricorn Group were lower following November 2021 than following November 2022 (Fig. 6). Exceptional November 2022 settlement occurred despite a split spawning event in 2022, which divided the total reproductive effort between November and December spawnings. This potentially strengthens our inference that the model did indeed predict true differences in hydrodynamic contributions to total propagule input between November 2021 and November 2022. In contrast, the model displayed poor performance at predicting larval influx. Comparisons of measured larval densities versus modelled larval density predictions demonstrated a poor fit (Fig. 3a). To the best of our knowledge, larval density validation of connectivity models using field measurements is limited to two other studies. Water column coral larvae density was found to correlate with model predictions generated for a lagoonal platform reef in the central GBR (Black, 1988; Willis and Oliver, 1988). However, in the following year, a different hydrodynamic model of the same reef did not generate predictions that correlated with water column larval densities (Oliver et al., 1992). There is a clear challenge in sampling coral larvae in the water column and relating their abundances to those predicted by biophysical particle models.

Larval abundances may be affected by stochastic processes (e.g. clumping: Alldredge and Hamner, 1980; Epifanio and Tilburg, 2008) and we explored the potential impact of this on our sampling through two tests. High resolution timeseries of larval abundance versus coral settlement indicated a relatively well-matched relationship at three sites. At a fourth site, an apparent peak in settlement prior to a peak in measured larval abundance suggested that the first appearance of this peak had been missed. A dataset in which tows were replicated six times per day from which we generated all possible single-daily timepoint timeseries of larval abundances, showed wide variation in the resulting timeseries means at sites with strong larval peaks (Fig. 8). This demonstrates that observational uncertainties and limitations exist and that they could reduce the power of the observational larval abundance dataset for model validation.

Settler densities may, in one respect, be a better indicator of connectivity as settlement tiles continually "sample" over the time period

following spawning (until their retrieval), whilst larval tows allow only short sampling events over the same period. On the other hand, the process of settlement presents additional filters, such as benthic compositions that can induce or discourage metamorphosis (Arnold and Steneck, 2011; Doropoulos et al., 2017; Price, 2010), which may obfuscate the true connectivity signal. Additionally, high vulnerability to mortality occurs immediately following settlement, with Type III exponential decays typically observed across all benthic invertebrates (Gosselin and Qian, 1997), including corals (e.g. Doropoulos et al., 2022; Doropoulos et al., 2016), adding another source of noise between measurements of larval supply and settlement. Although highly significant, the variability in the relationship between measured larval arrival and settlement (e.g. Wistari_S in 2021, Fig. 3c) illustrates that at least some sources of stochasticity are in operation, whether they be related to larval sampling issues or biological filters on settlement and early post-settlement survival (Pineda et al., 2009).

While the model shows poor to fair performance in quantitative predictions of larval supply and settlement (Fig. 3a and b), there is a remarkable qualitative agreement when assessing each reef separately and identifying which sector of the reef is a high or low receiving environment. Moreover, across the three spawning events, the sectors retain their relative characteristics (Fig. 6). This result suggests that the hydrodynamic circulation around the reef is selectively delivering the larvae to specific sectors in a realistic manner. The quantitative predictive power might be impacted by under-representation of local retention, as this is often not well characterised in biophysical particle tracking studies (Dauhajre et al., 2019; Riginos et al., 2019). However, Wolanski and Kingsford (2014) showed that the presence of tidal phase eddies and a small sticky water effect together generated only a mild level of local retention of larvae in the central Capricorn Group, lower than that expected in denser reef matrices common in other parts of the GBR. The qualitative agreement when assessing quadrants around individual reefs, and representation of repeated inter-year patterns, suggests that the high-resolution model is quite successful at identifying hydrodynamic regimes that constrain the spatial patterns of larval supply around the reef.

Although none of the sensitivity tests resulted in highly improved quantitative model versus observation comparisons, they revealed many useful insights into the parameter choices made. Connolly and Baird's (2010) equations for *A. valida* performed slightly better than the reference case, Moneghetti et al.'s (2019) equations for *A. tenuis*. This result may simply reflect the focus of our study on the first 10 d of dispersal as both survival equations deliver similar results during this stage. Ideally, a range of competency and mortality equations covering a range of coral taxa would be utilised (see Randall et al., 2024) to cover a broader suite of model taxa, although *Acropora* and Merulinidae are those with the best information available, and *Acropora* is the most modelled taxon in the Indo-Pacific (Figueiredo et al., 2022; Faryuni et al., 2024; Saint-Amand et al., 2023; Connolly and Baird, 2010; Bento et al., 2021).

Changing the size and shape of the receiving polygons generated the most dramatic results of all sensitivity tests. Setting the receiving polygon to the five hydrodynamic model grid cells containing each field station resulted in a large drop in prediction performance. This was driven by extremely high modelled connectivity values at Sykes Reef. In contrast, setting the receiving polygons to the three hydrodynamic model grid cells parallel to the reef crest at each sampling station resulted in model performance similar to the level of the original set of receiving polygons. Setting the receiving polygon to a circular polygon of 210 m diameter centred at each sampling station, theoretically the most realistic scale mimicking the field sampling conditions, resulted in a poor fit, generated by zero modelled connectivity values at two sites (Heron_SW and Heron_S). The reasons for these zero values when using the circular polygons were undetermined.

Connectivity model validation should ideally validate the connectivity matrix (the presence/absence and strength of connections between all pairs of source and sink nodes in the network). The connectivity matrix is a minimal but complete set of information describing the modelled connectivity network, and has applied uses in a range of circumstances, including optimal decision-making for environmental management and restoration (Beger et al., 2022). Our validation approach – propagule census – does not assess the connectivity matrix directly but rather assesses whether the biophysical model used to produce the matrix can correctly predict particle influx at a sample of sites. The problem with this approach is that if the predictive ability of the biophysical model is moderately low, as in our case, we cannot use that information to identify which pairwise connections within the matrix are incorrect, or too weak or too strong, and therefore where the model can be improved to generate practical improvements to the connectivity matrix.

Whilst validation of the underlying connectivity matrix is an ideal form of validation, there are two alternative approaches that are potentially useful. The first is the validation of absolute fluxes of particles into particular sites. This approach was used by Thomas et al. (2012) who used measured larvae densities of pearl oyster on the day of spawning to initialise particle tracking in a connectivity model of a French Polynesian atoll. Whilst fluxes of larvae simulated by the subsequent modelling were incorrect at many sampling stations, two stations demonstrated a strong matchup between timeseries of modelled and measured fluxes. To apply this approach to coral connectivity modelling, good estimates of larval output from source reefs is required, a difficult though not unfeasible undertaking. Indeed, broad field sampling to quantify how larval output varies across colonies, species and habitats within our source reefs would allow characterisation of geographic variation in larval output, allowing our assumption of uniform larval output per unit area of coral cover to be superseded.

The second is the validation of *relative* strengths of connections in the connectivity matrix – that is, the connections that result from physical forcings alone without taking into account any biological factors. This "weaker" form of connectivity validation is still useful for operational environmental decision making, as some ecological models are capable of predicting biological aspects of dispersal, such as the number of larvae released, and so do not require the connectivity matrix to reflect this (Bozec et al., 2022). Matrix validation then becomes purely a matter of physical oceanographic measurement (Lee et al., 1992), as opposed to a validation of biophysical processes that are (as experienced in this study) inherently harder to measure accurately.

In summary, we deployed and validated a high-resolution connectivity model of larval supply and settlement across three reefs in a characteristic offshore reef system in the southern GBR. Many aspects of the underlying hydrodynamic model correlated well with *in situ* instrumentation, while a few did not. In general, the predictions of larval abundance in the water column were not correlated with observational datasets, while observations of larval settlement were correlated with predictions but were highly variable. In the case of larval abundance, natural stochasticity may have introduced an additional confounding effect, however, coral settlement provided a signal for model validation that was less affected by this issue. This suggests that additional ecological and biophysical parameters are affecting the predictive ability of the particle modelling at the fine scale of spatial resolution being tested. Importantly, while many studies have applied connectivity modelling to inform marine spatial conservation planning (Balbar and Metaxas, 2019), these remain untested and should be validated alongside operationalisation to improve on the efficacy of zoning. Similarly, while it has been proposed that connectivity be incorporated for restoration activities (e.g. Doropoulos and Babcock, 2018), the scale of restoration activities are typically >1/10 ha to <10 ha and therefore caution needs to be applied to the use of such high-resolution models for decision making until they are adequately validated (Ladd and Burkepile, 2018).

Model validation may benefit from developing a quantitative framework to guide the design of future connectivity validation attempts. This framework should unite the spatial scale, temporal scale

and location-specific aspects of hydrodynamic model error, propagule variability, and the error tolerance of the connectivity end use. A hydrodynamic model's structure, resolution and computational implementation means that its performance at simulating particular fluid phenomena or bathymetric features may differ. Larval settlement patterns may show spatial consistency around some features (physical, e.g. bathymetry; or ecological, e.g. community type) and high variability in other contexts. The use of connectivity in ecological models for decision support may have a low error tolerance due to the many dependencies of the socio-ecological context of the model, whilst some other uses may have more tolerance for error. The location, scales and replication required for biological sampling to validate connectivity can be informed by a formal experimental design process that considers the hydrodynamic model error, natural propagule variability and use-case error tolerance.

CRediT authorship contribution statement

Robert A.B. Mason: Writing – review & editing, Writing – original draft, Visualization, Validation, Software, Project administration, Methodology, Investigation, Formal analysis, Data curation, Conceptualization. **Clothilde Langlais:** Writing – review & editing, Visualization, Validation, Supervision, Software, Project administration, Methodology, Investigation, Formal analysis, Data curation, Conceptualization. **Julian Uribe-Palomino:** Validation, Methodology, Investigation, Data curation. **Mark Tonks:** Project administration, Methodology, Investigation, Data curation. **Frank Coman:** Methodology, Investigation, Data curation. **Severine Choukroun:** Writing – review & editing, Software, Methodology. **Javier Porobic:** Writing – review & editing, Software, Methodology. **Christopher Doropoulos:** Writing – review & editing, Validation, Supervision, Software, Project administration, Methodology, Investigation, Funding acquisition, Formal analysis, Data curation, Conceptualization.

Data availability statement

The datasets used for this study are deposited in the CSIRO Data Access Portal: https://data.csiro.au/collection/62876 and https://data.csiro.au/collection/62652. Code used in the analysis is archived at the following link: https://bitbucket.csiro.au/projects/ECORRAP2S1/repos/capricorn_connectivity_2021_2022/browse.

Declaration of competing interest

The authors declare that they have no known competing financial interests or personal relationships that could have appeared to influence the work reported in this paper.

Acknowledgements

The authors would like to acknowledge the Port Curtis Coral Coast Traditional Owners of the Capricorn-Bunker region, the Byelle, Gooreng Gooreng, Gurang and Taribelang Bunda First Nations people, for permission to work and collect samples in their Sea Country. We would like to thank Morane Le Nohaic, Pascal Craw, Melanie Orr, Kinam Salee, Devin Rowell, Elizabeth Buccheri, Leah Soo, Costanza Algieri, Madeleine Weir, Beau de Groot, Gidarjil Corporation and Heron Island Research Station staff for support in the field. Bec Gorton, John Andrewartha and Richard Thomson are thanked for assistance with hydrodynamic and connectivity modelling. Katharina Fabricius and Sam Noonan are thanked for providing ADCP data and for loans of drag-tilt current sensors. Peter Mumby, Russell Babcock, Anthony Richardson, and Sharon Tickell are thanked for thoughtful discussions. Karlo Hock is thanked for help with reuse of whole-of-GBR connectivity data. This work was supported by the EcoRRAP subprogram (https://gbrrestoration.org/program/ecorrap/) that is part of the Reef Restoration and Adaptation Program (https://gbrrestoration.org/). The Reef Restoration and Adaptation Program is funded by the partnership between the Australian Government's Reef Trust and the Great Barrier Reef Foundation. The funders had no role in study design, data collection and analysis, decision to publish, or preparation of the manuscript. The authors declare no conflict of interest.

Appendix A. Supplementary data

Supplementary data to this article can be found online at https://doi.org/10.1016/j.ecss.2025.109506.

Data availability

Data have been placed in online repositories which will be made publicly accessible upon manuscript publication.

References

Abdul Wahab, M.A., Ferguson, S., Snekkevik, V.K., et al., 2023. Hierarchical settlement behaviours of coral larvae to common coralline algae. Sci. Rep. 13 (1), 5795. https://doi.org/10.1038/s41598-023-32676-4.

Alldredge, A.L., Hamner, W.M., 1980. Recurring aggregation of Zooplankton by a tidal current. Estuar. Coast. Mar. Sci. 10 (1), 31–37. https://doi.org/10.1016/S0302-3524(80)80047-8.

Almany, G.R., Berumen, M.L., Thorrold, S.R., Planes, S., Jones, G.P., 2007. Local replenishment of coral reef fish populations in a marine reserve. Science 316 (5825), 742–744. https://doi.org/10.1126/science.1140597.

Andrews, J.C., Gay, S., Sammarco, P.W., 1988. Influence of circulation on self-seeding patterns at Helix reef, Great Barrier Reef. In: Choat, J.H., Barnes, D.J., Borowitzka, M.A., et al. (Eds.), Proceedings of the 6th International Coral Reef Symposium, vol. 2, pp. 469–474.

Arnold, S.N., Steneck, R.S., 2011. Settling into an increasingly hostile world: the rapidly closing "Recruitment Window" for corals. PLoS One 6 (12), e28681. https://doi.org/10.1371/journal.pone.0028681.

Babcock, R.C., Bull, G.D., Harrison, P.L., et al., 1986. Synchronous spawnings of 105 scleractinian coral species on the Great Barrier Reef. Mar. Biol. 90 (3), 379–394. https://doi.org/10.1007/bf00428562.

Babcock, R.C., Baird, A.H., Piromvaragorn, S., Thomson, D.P., Willis, B.L., 2003. Identification of scleractinian coral recruits from Indo-Pacific reefs. Zool. Stud. 42 (1), 211–226.

Baird, A.H., Babcock, R.C., 2000. Morphological differences among three species of newly settled pocilloporid coral recruits. Coral Reefs 19 (2), 179–183. https://doi.org/10.1007/PL00006955.

Baird, M.E., Wild-Allen, K.A., Parslow, J., et al., 2020. CSIRO Environmental Modelling Suite (EMS): scientific description of the optical and biogeochemical models (vB3p0). Geosci. Model Dev. 13 (9), 4503–4553. https://doi.org/10.5194/gmd-13-4503-2020.

Balbar, A.C., Metaxas, A., 2019. The current application of ecological connectivity in the design of marine protected areas. Glob. Ecol. Conserv. 17, e00569. https://doi.org/10.1016/j.gecco.2019.e00569.

Baums, I.B., Paris, C.B., Chérubin, L.M., 2006. A bio-oceanographic filter to larval dispersal in a reef-building coral. Limnol. Oceanogr. 51 (5), 1969–1981. https://doi.org/10.4319/lo.2006.51.5.1969.

Beger, M., Metaxas, A., Balbar, A.C., et al., 2022. Demystifying ecological connectivity for actionable spatial conservation planning. Trends Ecol. Evol. 37 (12), 1079–1091. https://doi.org/10.1016/j.tree.2022.09.002.

Beletsky, D., Beletsky, R., Rutherford, E.S., et al., 2017. Predicting spread of aquatic invasive species by lake currents. J. Gt. Lakes Res. 43 (3), 14–32. https://doi.org/10.1016/j.jglr.2017.02.001.

Bento, R., Cavalcante, G., Mateos-Molina, D., Riegl, B., Bejarano, I., 2021. Recruitment and larval connectivity of a remnant Acropora community in the Arabian Gulf, United Arab Emirates. Coral Reefs 40 (6), 1889–1898. https://doi.org/10.1007/s00338-021-02187-7.

Bode, M., Leis, J.M., Mason, L.B., et al., 2019. Successful validation of a larval dispersal model using genetic parentage data. PLoS Biol. 17 (7), e3000380. https://doi.org/10.1371/journal.pbio.3000380.

Bode, M., Stewart, O., Choukroun, S., Wolanski, E., Kingsford, M.J., 2024. Incorporating biophysical larval dispersal simulations into coral reef conservation decision-making. In: Wolanski, E., Kingsford, M.J. (Eds.), Oceanographic Processes of Coral Reefs: Physical and Biological Links in the Great Barrier Reef, second ed. CRC Press, pp. 272–281.

Bozec, Y.M., Hock, K., Mason, R.A.B., et al., 2022. Cumulative impacts across Australia's Great Barrier Reef: a mechanistic evaluation. Ecol. Monogr. 92 (1), e01494. https://doi.org/10.1002/ecm.1494.

Brazeau, D.A., Sammarco, P.W., Gleason, D.F., 2005. A multi-locus genetic assignment technique to assess sources of Agaricia agaricites larvae on coral reefs. Mar. Biol. 147 (5), 1141–1148. https://doi.org/10.1007/s00227-005-0022-5.

Brooks, M.E., Kristensen, K., Benthem, K J van, et al., 2017. glmmTMB balances speed and flexibility among packages for zero-inflated generalized Linear mixed modeling. R J. 9 (2), 378–400. https://doi.org/10.32614/RJ-2017-066.

Bruyère, O., Chauveau, M., Le Gendre, R., Liao, V., Andréfouët, S., 2023. Larval dispersal of pearl oysters Pinctada margaritifera in the Gambier Islands (French Polynesia) and exploring options for adult restocking using in situ data and numerical modelling. Mar. Pollut. Bull. 192, 115059. https://doi.org/10.1016/j.marpolbul.2023.115059.

Cavalcante, G., Vieira, F., Mortensen, J., et al., 2020. Chapter eight - biophysical model of coral population connectivity in the Arabian/Persian Gulf. In: Riegl, B.M. (Ed.), Advances in Marine Biology, vol. 87: Population Dynamics of the Reef Crisis. Academic Press, pp. 193–221. https://doi.org/10.1016/bs.amb.2020.07.001.

Cecino, G., Treml, E.A., 2021. Local connections and the larval competency strongly influence marine metapopulation persistence. Ecol. Appl. 31 (4), e02302. https://doi.org/10.1002/eap.2302.

Black, K.P., 1988. The relationship of reef hydrodynamics to variations in numbers of planktonic larvae on and around coral reefs. In: Choat, J.H., Barnes, D., Borowitzka, M.A., et al. (Eds.), Proceedings of the 6th International Coral Reef Symposium, Australia, 2, pp. 125–130.

Condie, S.A., Hepburn, M., Mansbridge, J., 2012. Modelling and visualisation of connectivity on the Great Barrier Reef. In: Yellowlees, D., Hughes, T.P. (Eds.).

Connolly, S.R., Baird, A.H., 2010. Estimating dispersal potential for marine larvae: dynamic models applied to scleractinian corals. Ecology 91 (12), 3572–3583. https://doi.org/10.1890/10-0143.1.

Cowen, R.K., Sponaugle, S., 2009. Larval dispersal and marine population connectivity. Ann. Rev. Mar. Sci. 1 (1), 443–466. https://doi.org/10.1146/annurev.marine.010908.163757.

Cowen, R., Gawarkiewicz, G., Pineda, J., Thorrold, S., Werner, F., 2007. Population connectivity in marine systems: an overview. Oceanography (Wash. D. C.) 20 (3), 14–21. https://doi.org/10.5670/oceanog.2007.26.

Dauhajre, D.P., McWilliams, J.C., Renault, L., 2019. Nearshore lagrangian connectivity: submesoscale influence and resolution sensitivity. J. Geophys. Res. Oceans 124 (7), 5180–5204. https://doi.org/10.1029/2019JC014943.

Doropoulos, C., Babcock, R.C., 2018. Harnessing connectivity to facilitate coral restoration. Front. Ecol. Environ. 16 (10), 558–559. https://doi.org/10.1002/fee.1975.

Doropoulos, C., Roff, G., Bozec, Y., Zupan, M., Werminghausen, J., Mumby, P.J., 2016. Characterizing the ecological trade-offs throughout the early ontogeny of coral recruitment. Ecol. Monogr. 86 (1), 20–44. https://doi.org/10.1890/15-0668.1.

Doropoulos, C., Roff, G., Visser, M.S., Mumby, P.J., 2017. Sensitivity of coral recruitment to subtle shifts in early community succession. Ecology 98 (2), 304–314. https://doi.org/10.1002/ecy.1663.

Doropoulos, C., Gómez-Lemos, L.A., Salee, K., et al., 2022. Limitations to coral recovery along an environmental stress gradient. Ecol. Appl. 32 (3), e2558. https://doi.org/10.1002/eap.2558.

Epifanio, C.E., Tilburg, C.E., 2008. Transport of blue crab larvae in the middle Atlantic bight: a wet and windy journey. J. Mar. Res. 66 (6), 723–749. https://doi.org/10.1357/002224008788064586.

Faryuni, I.D., Saint-Amand, A., Dobbelaere, T., et al., 2024. Assessing coral reef conservation planning in Wakatobi National Park (Indonesia) from larval connectivity networks. Coral Reefs 43 (1), 19–33. https://doi.org/10.1007/s00338-023-02443-y.

Figueiredo, J., Thomas, C.J., Deleersnijder, E., et al., 2022. Global warming decreases connectivity among coral populations. Nat. Clim. Change 12 (1), 83–87. https://doi.org/10.1038/s41558-021-01248-7.

Gawarkiewicz, G., Monismith, S., Largier, J., 2007. Observing larval transport processes affecting population connectivity: progress and challenges. Oceanography (Wash. D. C.) 20 (3), 40–53. https://doi.org/10.5670/oceanog.2007.28.

Golbuu, Y., Wolanski, E., Idechong, J.W., et al., 2012. Predicting coral recruitment in Palau's complex reef archipelago. PLoS One 7 (11), e50998. https://doi.org/10.1371/journal.pone.0050998.

Gosselin, L., Qian, P., 1997. Juvenile mortality in benthic marine invertebrates. Mar. Ecol. Prog. Ser. 146, 265–282. https://doi.org/10.3354/meps146265.

Gouezo, M., Wolanski, E., Critchell, K., et al., 2021. Modelled larval supply predicts coral population recovery potential following disturbance. Mar. Ecol. Prog. Ser. 661, 127–145. https://doi.org/10.3354/meps13608.

Gouezo, M., Langlais, C., Beardsley, J., et al., 2025. Going with the flow: leveraging reef-scale hydrodynamics for upscaling larval-based restoration. Ecol. Appl. 35, e70020. https://doi.org/10.1101/2024.11.12.623286.

Gourlay, M.R., Colleter, G., 2005. Wave-generated flow on coral reefs—an analysis for two-dimensional horizontal reef-tops with steep faces. Coast. Eng. 52 (4), 353–387. https://doi.org/10.1016/j.coastaleng.2004.11.007.

Grimaldi, C.M., Lowe, R.J., Benthuysen, J.A., et al., 2022. Hydrodynamic drivers of fine-scale connectivity within a coral reef atoll. Limnol. Oceanogr. 67 (10), 2204–2217. https://doi.org/10.1002/lno.12198.

He, D., Ma, Y., Dong, G., Perlin, M., 2022. A numerical investigation of wave and current fields along bathymetry with porous media. Ocean Eng. 244, 110333. https://doi.org/10.1016/j.oceaneng.2021.110333.

Hock, K., Wolff, N.H., Beeden, R., et al., 2016. Controlling range expansion in habitat networks by adaptively targeting source populations. Conserv. Biol. 30 (4), 856–866. https://doi.org/10.1111/cobi.12665.

Hock, K., Doropoulos, C., Gorton, R., Condie, S.A., Mumby, P.J., 2019. Split spawning increases robustness of coral larval supply and inter-reef connectivity. Nat. Commun. 10 (1), 3463. https://doi.org/10.1038/s41467-019-11367-7.

Jell, J.S., Flood, P.G., 1978. Guide to the geology of reefs of the Capricorn and Bunker groups, Great Barrier Reef Province. Pap. Dep. Geol. Univ. Qld. 8 (3), 1–85.

Kleptsova, O., Stelling, G.S., Pietrzak, J.D., 2010. An accurate momentum advection scheme for a z-level coordinate models. Ocean Dyn. 60 (6), 1447–1461. https://doi.org/10.1007/s10236-010-0350-y.

Klingbeil, K., Lemarié, F., Debreu, L., Burchard, H., 2018. The numerics of hydrostatic structured-grid coastal ocean models: state of the art and future perspectives. Ocean Model. 125, 80–105. https://doi.org/10.1016/j.ocemod.2018.01.007.

Ladd, M.C., Burkepile, D.E., 2018. A response to Doropoulos and Babcock. Front. Ecol. Environ. (16), 559–560.

Lee, T.N., Rooth, C., Williams, E., McGowan, M., Szmant, A.F., Clarke, M.E., 1992. Influence of Florida current, gyres and wind-driven circulation on transport of larvae and recruitment in the Florida Keys coral reefs. Cont. Shelf Res. 12 (7), 971–1002. https://doi.org/10.1016/0278-4343(92)90055-O.

Leichter, J., Shellenbarger, G., Genovese, S., Wing, S., 1998. Breaking internal waves on a Florida (USA) coral reef: a plankton pump at work? Mar. Ecol. Prog. Ser. 166, 83–97. https://doi.org/10.3354/meps166083.

Lin, B., Falconer, R.A., 1997. Three-dimensional layer-integrated modelling of estuarine flows with flooding and drying. Estuar. Coast. Shelf Sci. 44 (6), 737–751. https://doi.org/10.1006/ecss.1996.0158.

Luo, M., Khayyer, A., Lin, P., 2021. Particle methods in ocean and coastal engineering. Appl. Ocean Res. 114, 102734. https://doi.org/10.1016/j.apor.2021.102734.

Lyons, M.B., Roelfsema, C.M., Kennedy, E.V., et al., 2020. Mapping the world's coral reefs using a global multiscale earth observation framework. Remote Sens. Ecol. Conserv. 6 (4), 557–568. https://doi.org/10.1002/rse2.157.

McCarroll, R.J., Scott, T., King, E.V., et al., 2021. Modelling regional and local-scale larval seeding strategies for abalone (H. midae) ranching in South Africa. Aquaculture 540, 736668. https://doi.org/10.1016/j.aquaculture.2021.736668.

Moneghetti, J., Figueiredo, J., Baird, A.H., Connolly, S.R., 2019. High-frequency sampling and piecewise models reshape dispersal kernels of a common reef coral. Ecology 100 (8), e02730. https://doi.org/10.1002/ecy.2730.

Mongin, M., Baird, M., 2014. The interacting effects of photosynthesis, calcification and water circulation on carbon chemistry variability on a coral reef flat: a modelling study. Ecol. Model. 284, 19–34. https://doi.org/10.1016/j.ecolmodel.2014.04.004.

Mongin, M., Baird, M.E., Hadley, S., Lenton, A., 2016. Optimising reef-scale CO_2 removal by seaweed to buffer ocean acidification. Environ. Res. Lett. 11 (3), 034023. https://doi.org/10.1088/1748-9326/11/3/034023.

Nolasco, R., Gomes, I., Peteiro, L., et al., 2018. Independent estimates of marine population connectivity are more concordant when accounting for uncertainties in larval origins. Sci. Rep. 8 (1), 2641. https://doi.org/10.1038/s41598-018-19833-w.

Oliver, J.K., King, B.A., Willis, B.L., Babcock, R.C., Wolanski, E., 1992. Dispersal of coral larvae from a lagoonal reef—II. Comparisons between model predictions and observed concentrations. Cont. Shelf Res. 12 (7), 873–889. https://doi.org/10.1016/0278-4343(92)90049-P.

Pineda, J., Reyns, N.B., Starczak, V.R., 2009. Complexity and simplification in understanding recruitment in benthic populations. Popul. Ecol. 51, 17–32.

Price, N., 2010. Habitat selection, facilitation, and biotic settlement cues affect distribution and performance of coral recruits in French Polynesia. Oecologia 163 (3), 747–758. https://doi.org/10.1007/s00442-010-1578-4.

Puri, K., Dietachmayer, G., Steinle, P., et al., 2013. Implementation of the initial ACCESS numerical weather prediction system. Aust. Meteorol. Oceanogr. J. 63 (2), 265–284. https://doi.org/10.22499/2.6302.001.

Quigley, K.M., Bay, L.K., van Oppen, M.J.H., 2019. The active spread of adaptive variation for reef resilience. Ecol. Evol. 9 (19), 11122–11135. https://doi.org/10.1002/ece3.5616.

Ramirez-Romero, E., Amores, A., Diaz, D., et al., 2023. Atmospheric–ocean coupling drives prevailing and synchronic dispersal patterns of marine species with long pelagic durations. Sci. Rep. 13 (1), 2366. https://doi.org/10.1038/s41598-023-29543-7.

Randall, C.J., Giuliano, C., Stephenson, B., et al., 2024. Larval precompetency and settlement behaviour in 25 Indo-Pacific coral species. Commun. Biol. 7 (1), 142. https://doi.org/10.1038/s42003-024-05824-3.

Riginos, C., Hock, K., Matias, A.M., Mumby, P.J., van Oppen, M.J.H., Lukoschek, V., 2019. Asymmetric dispersal is a critical element of concordance between biophysical dispersal models and spatial genetic structure in Great Barrier Reef corals. Divers. Distrib. 25 (11), 1684–1696. https://doi.org/10.1111/ddi.12969.

Roelfsema, C.M., Lyons, M.B., Castro-Sanguino, C., et al., 2021. How much shallow coral habitat is there on the Great Barrier Reef? Remote Sens. 13 (21), 4343. https://doi.org/10.3390/rs13214343.

Rogers, J.S., Monismith, S.G., Fringer, O.B., Koweek, D.A., Dunbar, R.B., 2017. A coupled wave-hydrodynamic model of an atoll with high friction: mechanisms for flow, connectivity, and ecological implications. Ocean Model. 110, 66–82. https://doi.org/10.1016/j.ocemod.2016.12.012.

Rossa, A., Nurmi, P., Ebert, E., 2008. Overview of methods for the verification of quantitative precipitation forecasts. In: Michaelides, S. (Ed.), Precipitation: Advances in Measurement, Estimation and Prediction. Springer, pp. 419–452. https://doi.org/10.1007/978-3-540-77655-0_16.

Rossi, V., Ser-Giacomi, E., López, C., Hernández-García, E., 2014. Hydrodynamic provinces and oceanic connectivity from a transport network help designing marine reserves. Geophys. Res. Lett. 41 (8), 2883–2891. https://doi.org/10.1002/2014GL059540.

Saint-Amand, A., Lambrechts, J., Hanert, E., 2023. Biophysical models resolution affects coral connectivity estimates. Sci. Rep. 13 (1), 9414. https://doi.org/10.1038/s41598-023-36158-5.

Schiller, A., Brassington, G.B., Oke, P., et al., 2020. Bluelink ocean forecasting Australia: 15 years of operational ocean service delivery with societal, economic and environmental benefits. J. Oper. Oceanogr. 13 (1), 1–18. https://doi.org/10.1080/1755876X.2019.1685834.

Schlaefer, J., Carter, A., Choukroun, S., et al., 2022. Marine plant dispersal and connectivity measures differ in their sensitivity to biophysical model parameters. Environ. Model. Software 149, 105313. https://doi.org/10.1016/j.envsoft.2022.105313.

Shaver, E.C., McLeod, E., Hein, M.Y., et al., 2022. A roadmap to integrating resilience into the practice of coral reef restoration. Glob. Change Biol. 28 (16), 4751–4764. https://doi.org/10.1111/gcb.16212.

Simons, R.D., Siegel, D.A., Brown, K.S., 2013. Model sensitivity and robustness in the estimation of larval transport: a study of particle tracking parameters. J. Mar. Syst. 119–120, 19–29. https://doi.org/10.1016/j.jmarsys.2013.03.004.

Steven, A.D.L., Baird, M.E., Brinkman, R., et al., 2019. eReefs: an operational information system for managing the Great Barrier Reef. J. Oper. Oceanogr. 12 (Suppl. 2), S12–S28. https://doi.org/10.1080/1755876X.2019.1650589.

Storlazzi, C.D., van Ormondt, M., Chen, Y.L., Elias, E.P.L., 2017. Modeling fine-scale coral larval dispersal and interisland connectivity to help designate mutually-supporting coral Reef marine protected areas: insights from Maui Nui, Hawaii. Front. Mar. Sci. 4, 381. https://www.frontiersin.org/articles/10.3389/fmars.2017.00381.

Swearer, S.E., Treml, E.A., Shima, J.S., 2019. A Review of Biophysical Models of Marine Larval Dispersal. In: Hawkins, S.J., Allcock, A.L., Bates, A.E., et al. (Eds.), Oceanography and Marine Biology: An Annual Review, 57. CRC Press, pp. 325–356. doi:10.1201/9780429026379-7.

Tay, Y.C., Guest, J.R., Chou, L.M., Todd, P.A., 2011. Vertical distribution and settlement competencies in broadcast spawning coral larvae: implications for dispersal models. J. Exp. Mar. Biol. Ecol. 409 (1–2), 324–330. https://doi.org/10.1016/j.jembe.2011.09.013.

Thomas, Y., Le Gendre, R., Garen, P., Dumas, F., Andréfouët, S., 2012. Bivalve larvae transport and connectivity within the Ahe atoll lagoon (Tuamotu Archipelago), with application to pearl oyster aquaculture management. Mar. Pollut. Bull. 65 (10–12), 441–452. https://doi.org/10.1016/j.marpolbul.2011.12.027.

Thomson, D.P., Babcock, R.C., Evans, R.D., et al., 2021. Coral larval recruitment in north-western Australia predicted by regional and local conditions. Mar. Environ. Res. 168, 105318. https://doi.org/10.1016/j.marenvres.2021.105318.

Tonks, M., Coman, F., Mason, R., Uribe-Palomino, J., Woods, D., Doropoulos, C., 2023. Plankton Tow Sampling to Estimate Coral Larvae Relative Abundance – Standard Operating Procedure, CSIRO, 20 pp.

Uchiyama, Y., Odani, S., Kashima, M., Kamidaira, Y., Mitarai, S., 2018. Influences of the Kuroshio on interisland remote connectivity of corals across the Nansei Archipelago in the East China Sea. J. Geophys. Res. Oceans 123 (12), 9245–9265. https://doi.org/10.1029/2018JC014017.

van Sebille, E., Griffies, S.M., Abernathey, R., et al., 2018. Lagrangian ocean analysis: fundamentals and practices. Ocean Model. 121, 49–75. https://doi.org/10.1016/j.ocemod.2017.11.008.

Werner, F., Cowen, R., Paris, C., 2007. Coupled biological and physical models: present capabilities and necessary developments for future studies of population connectivity. Oceanography (Wash. D. C.) 20 (3), 54–69. https://doi.org/10.5670/oceanog.2007.29.

Willis, B.L., Oliver, J.K., 1988. Distribution of Coral Eggs and Larvae in the Central Section of the Great Barrier Reef Marine Park Following the Annual Mass Spawning of Corals. Final Report to the Great Barrier Reef Marine Park Authority. 49 pages.

Wolanski, E., Kingsford, M.J., 2014. Oceanographic and behavioural assumptions in models of the fate of coral and coral reef fish larvae. J. R. Soc. Interface 11 (98), 20140209. https://doi.org/10.1098/rsif.2014.0209.

Wood, S., Baums, I.B., Paris, C.B., Ridgwell, A., Kessler, W.S., Hendy, E.J., 2016. El Niño and coral larval dispersal across the eastern Pacific marine barrier. Nat. Commun. 7 (1), 12571. https://doi.org/10.1038/ncomms12571.

Zhibing, L., Zhongya, C., Zhiqiang, L., Xiaohua, W., Jianyu, H., 2022. A novel identification method for unrevealed mesoscale eddies with transient and weak features-Capricorn Eddies as an example. Remote Sens. Environ. 274, 112981. https://doi.org/10.1016/j.rse.2022.112981.